ABSORBER MATERIALS
FOR SOLAR THERMAL POWER PLANT

BY

GHAZI ZULHAZMI

A Thesis Presented to the
DEANSHIP OF GRADUATE STUDIES

KING FAHD UNIVERSITY OF PETROLEUM & MINERALS
DHAHRAN, SAUDI ARABIA

In Partial Fulfillment of the
Requirements for the Degree of

MASTER OF SCIENCE

In

MATERIALS SCIENCE AND ENGINEERING

DECEMBER 2017

KING FAHD UNIVERSITY OF PETROLEUM & MINERALS

DHAHRAN- 31261, SAUDI ARABIA

DEANSHIP OF GRADUATE STUDIES

This thesis, written by **GHAZI ZULHAZMI HERRY** under the direction of his thesis advisor and approved by his thesis committee, has been presented and accepted by the Dean of Graduate Studies, in partial fulfillment of the requirements for the degree of **MASTER OF SCIENCE IN MATERIALS SCIENCE & ENGINEERING.**

Dr. Amro M. Al Qutub
(Advisor)

Dr. Tahar Laoui
(Member)

Dr. Esmail M.A. Mokheimer
(Member)

Dr. Zuhair M. Gasem
Department Chairman

Dr. Salam A. Zummo
Dean of Graduate Studies

عمادة الدراسات العليا
DEANSHIP OF GRADUATE STUDIES

21/5/18
Date

بسم الله الرحمن الرحيم

Dedicated to

my beloved parents

Herry Rechnaidi and Saptawati

my darling

Parahita G. Kusumaningtyas

and

my brothers and sisters, all of them

ACKNOWLEDGMENTS

In the name of Allah, the Entirely Merciful, the Especially Merciful. I am most grateful to Allah for His blessing, grace, and guidance upon me for undertaking this thesis successfully. May peace and blessing be upon prophet Muhammad, his family, and his companions.

I would like to deeply thank the authority of Kingdom of Saudi Arabia and KFUPM for their unbelievable support and facilities provided to me for studying and completing my master degree in KFUPM.

My deep gratitude and appreciations always goes to Dr. Amro Al Qutub, Dr. Tahar Laoui, and Dr. Esmail Mokheimer for their never-ending support, guidance, encouragement, and advice to help me finished my master thesis.

I am highly grateful to all ME Dept. faculties and staffs, especially Dr. Zuhair Gasem, for his guidance and support therefore I could complete my degree.

I would like to express my heartfelt thanks to my parents, my wife, and all my brothers and sisters for their prayers, supports, and patience throughout my life. I am proud of you all.

Sincere thanks to Abdulhakeem, Ismaila Aliyu, Maajed Linjawi, Ahmad Al-Jabr, Mohammad Amin, Rangga Ganzar, Iqbal Balatif, Yusri Syahrir, Syarif R., Fandi O., and all my friends and colleagues, which cannot be mentioned one by one, who provided great company, supports, prayers, and memories. It is a gift to have you all.

TABLE OF CONTENTS

LIST OF TABLES

LIST OF FIGURES

ABSTRACT

Full Name : [Ghazi Zulhazmi]

Thesis Title : [Absorber Materials for Solar Thermal Power Plant]

Major Field : [Materials Science and Engineering]

Date of Degree : [December 2017]

Absorber material in solar thermal power plants transfers heat energy from concentrated solar light to the working fluid inside the receiver. Hence, analyzing and observing the absorber properties must take place in order to improve the heat transfer efficiency of the system. Several material properties should be considered, such as maximum working temperature, thermal conductivity, coefficient of thermal expansion, and resistance to thermal fatigue. In this research, the materials used are alumina (Al_2O_3), silicon carbide (SiC), and siliconized silicon carbide (SiSiC), all in foam structure. The research was a pilot project for a solar thermal power plant in the region. An experimental setup and a receiver were made to support this field of research later. The present work investigated material behavior under thermal fatigue to determine which materials have better resistance to thermal cycles and are more suitable as an absorber. A thermal fatigue experiment in an air environment was conducted for up to 200 cycles at 1073 K and 1273 K. Thermal conductivity measurement, phase analysis, and micro/macro structure were performed using the Modified Transient Plane Source method, XRD, EDS, SEM, and stereomicroscope, respectively. There were no significant changes in the results, neither before nor after the experiment, of thermal conductivity of all the samples. The results showed that only the Al_2O_3 sample developed micro-cracks during the experiment at 1073 K (observed by SEM) and edge-to-edge macro-cracks at 1273 K as observed by stereomicroscope. The phase analysis showed no compositional change after the experiment for all samples as confirmed by EDS and XRD analysis. Therefore, SiC and SiSiC showed better performance than Al_2O_3 for absorber application.

ملخص الرسالة

الإسم : غازي ذوالحزم

عنوان الرسالة : مواد امتصاص لمحطة الطاقة الحرارية الشمسية

التخصص : علم و هندسة المواد

تاريخ الدرجة : ديسمبر 2017

تقوم مواد الامتصاص في محطة الطاقة الحرارية الشمسية بنقل الطاقة الحرارية من الضوء الشمسي المركز إلى سائل التشغيل داخل جهاز الاستقبال. وبالتالي ، هناك حاجة لتحليل ومراقبة خصائص الامتصاص (مادة الامتصاص) بعد التطبيق لتحسين كفاءة نقل الحرارة في النظام. يجب مراعاة العديد من خواص المواد ، مثل درجة حرارة العمل القصوى، التوصيل الحراري، معامل التمدد الحراري، ومقاومة الاجهاد الحراري. المواد المستخدمة (SiSiC ؛)، و كربيد السيليكون السليكوني (SiC) ، كربيد السيليكون (Al_2O_3في هذه الدراسة هي الألومينا (كلها في بنية الرغوة. تم إجراء هذا البحث كإعداد أولي لمحطة طاقة حرارية شمسية. ستحلل المناقشة سلوك المواد المختلفة في نفس حالة الاجهاد الحراري. ومن ثم ، فإننا نعرف اي مادة تتمتع بمقاومة أفضل للدورات الحرارية لأنه سيستخدم في تطبيق ذو درجة 1273Kوأكثرها ملاءمة لهذا التطبيق. درجة الحرارة الهواء المستهدفة هي و 1073K حرارة عالية. التجارب التي أجريت هي اجهاد حراري يصل إلى 200 دورة في درجات حرارة مختلفة (تم استخدام تحليل الصور لتحليل التكوين .أيضا تم إجراء قياسات التوصيل الحراري قبل وبعد التجربة).1273K . أظهرت النتائج أن EDS و XRD و SEM) و stereomicroscope والتشكيل باستخدام المجهر التشريحي (عينة الألومينا فقط طورت شقوقًا صغرى أثناء التجربة عند 1073 كلفن وشقوق كبيرة من الحافة إلى الحافة عند و EDS 1273 كلفن. لم يتم العثور على أي تغيير تركيبي أثناء التجربة لجميع العينات كما تم تأكيده بواسطة تحليل) يقدمان أداءً أفضل من SiSiC)، و كربيد السيليكون السليكوني (SiC ولذلك ، فإن كربيد السيليكون (.XRD الألومينا لتطبيق الامتصاص.

CHAPTER 1

INTRODUCTION

Solar energy had been harnessed as a renewable energy source for more than 40 years. This resource is abundant, cost-free, and clean compare to other resources. Therefore, numerous researches were conducted to efficiently harness solar light and convert it into electricity. Solar light energy harnessed in two ways; first, utilizing its electromagnetic wavelength and the other using its heat radiation. The second commonly used in solar thermal power plants while the first one used in photovoltaic solar cells. Especially in the Kingdom of Saudi Arabia (KSA), the utilization of solar energy has become more promising because the country is located under the sun-belt area. The sun-belt is the area on earth that is exposed to more solar radiation than most other areas annually. KSA receives 2200 kWh/m^2/year while other countries (outside the sun-belt) receive 1000 kWh/m^2/year.[1,2]

A solar thermal power plant uses heat energy of solar light to heats up fluid then the fluid is blown into a gas turbine to drive the generator and produce electricity. There are different setups in the solar thermal power plant systems, which varied based on the way the energy concentrated and transferred. One of the established technologies is concentrated solar power (CSP) system. In CSP, the light is reflected and concentrated by the mirror to a focus area, which is called the receiver. The receiver is a system where the concentrated light, fluids, and the absorber interact together. Absorber is the heat

exchanger medium inside the receiver. The concentrated light heats up the absorber then the heat is transferred directly to the fluid that flows through the absorber. The schematic of the systems showed in the Figure 1.

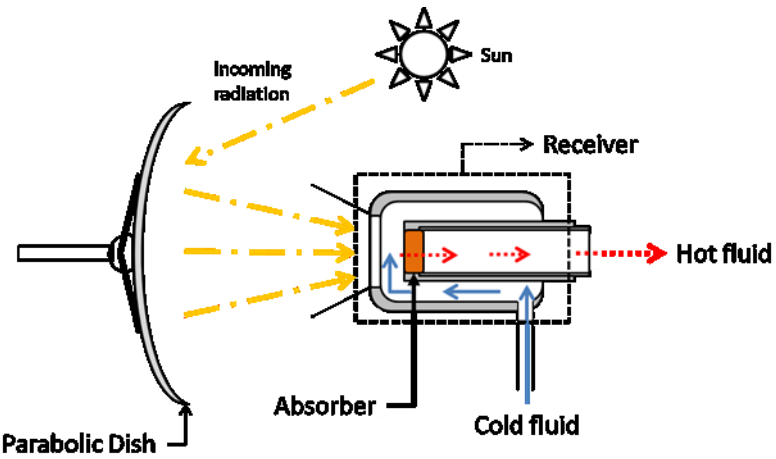

Figure 1 Schematic of a parabolic dish system and its receiver section.

The work presented in the thesis will focus its research to support the Parabolic Dish CSP system. It uses parabolic dish as the collector/concentrator and a volumetric receiver in the focus point of the dish. The ambient air used as the fluid. This system chosen because it has higher solar concentration ratio compare to the parabolic trough while it has simple design than the tower system.[3]

To increase the overall efficiency of the system, usually the solar thermal power plant combined with fuel power plant, which is called solar-hybid power plant. In this system, the heated air is burned with the fuel to get more energy, hence thermodynamically increasing the output energy of the generator. Therefore, as reported by Barigozzi *et al.*[4] and Sinai *et al.*[5], most of the researches on solar-hybrid power plants use 1000^{o}C as the target temperature for the outlet air temperature of the receiver.

For this system, the high-energy efficiency reached when the outlet temperature of air is high. One of the ways to increase the air temperature is maximizing the efficiency of heat transfer inside the receiver. The absorber, which typically has a foam structure, plays a vital role in this efficiency. Researches have been conducted to discover how to increase the absorber efficiency whether by modifying the structure or material. The integration with the gas turbine system requires the air that flows inside the receiver to be pressurized. Therefore, the receiver will be separated from the ambient environment thus a glass window should be used in the receiver.[6]

Since the high temperature of air will increase the efficiency, we decided that the target temperature for this study is 1000^{o}C (1273 K). In 1273 K, there are important properties of absorber that should be considered. Those properties are mechanical properties, chemical properties, optical properties (absorptivity and emissivity), thermal conductivity, specific surface area, and air permeability. Ceramic materials are the best candidate because typically it has high melting and operating temperature up to 1500^{o}C. Hence, analyzing material integrity, both mechanical and chemical stability, of the absorber is very important to ensure long-term sustainability of the absorber.

CHAPTER 2

ABSORBER AND PARABOLIC DISH

2.1 Literature Review

2.1.1 Absorber Material

One of the key components of the receiver is the absorber, the part where the heat transfer between the solar light and the fluids occur. Absorber performance plays a big role in the energy conversion efficiency of the system.

Numerous researches have been conducted to increase the efficiency and longevity of the absorber. The summary of studies, especially the efforts related to pressurized-fluid systems, is discussed in this chapter. However, some papers that used open-air systems are included in the discussion for a material perspective comparison.

The first attempt to study the pressurized-air receiver using ceramic material was done by Hanseth in 1976.[7] Their receiver consisted of a silicon carbide (SiC) honeycomb matrix as an absorber and a fused silica window. The temperature of the receiver achieved was 885^{o}C-1425^{o}C at full power without failure. Consequently, the heat efficiency estimation was 60% at 1120^{o}C and 80% at 885^{o}C. They show that ceramic material can be used as heat transfer medium in a high-flux solar exposure. The use of a window that separates the system from ambient air demonstrates the suitability of this system to be integrated within a gas turbine power plant.

Leuchsner in 1989[6] used a foam structure made from silicon nitride (Si_3N_4) ceramic coated with silicon carbide. After several experiments, the results were a power output of 2.5-3.7 kW, at a pressure of 4.2 bars, with 71% efficiency at an outlet air temperature 1050^{o}C. Then in 1993, they tried to make a higher capacity receiver that could deliver 500 kW. This receiver could reach maximum outlet air temperature of 960^{o}C and a pressure of 4.15 bars with efficiency 57.3% for energy delivered 92.4 kW. They had low efficiency because the average energy flux on the absorber was very low. It was noticed that the black coating used on the absorber surface has high reflectivity resulting in higher re-radiation loss. Therefore, a secondary concentrator was suggested to increase the flux and the use of low reflective coating should be considered to minimize re-radiation. The cracked window caused small leakage of air hence the air pressure could not exceed 4 bars. Generally, they found the importance of a window glass. It must be designed and considered very carefully to prevent heat loss, pressure loss, and ensure stability of the structure. They suggested using a domed glass window because it has lower reflection and better stress distribution during operation than a flat one.

The other research regarding absorber was performed by Karni *et al*., 1998[8]. They studied which absorber structures provide the best performance. They used three types of structure for the absorber: the porcupine, the foam, and the honeycomb made of Al_2O_3-SiO_2 (60% Al_2O_3). The receiver reached maximum outlet air temperature 940^{o}C while the absorber temperature was 1400^{o}C (maximum). Both maximum conditions were achieved using the porcupine structure, because the structure provides convective and radiative energy transport between the matrix elements, thereby alleviating the development of turbulence. The porcupine structure can sustain and transports much

higher energy fluxes compared to other structures. The foam and honeycomb structure reached high temperature with low outlet air temperature. After the experiment, both of them had localized damage in the structure. Karni *et al.* concluded that the damage occurred because the absorber experienced local overheating, so it partly cracked and melted. They also noticed that the effect of the absorber surface color to the efficiency was minimal compared to the structure effect.

The porcupine designed by Karni *et al.*[8] was applied by Kribus *et al.*[9] on big receiver. They reached higher absorber temperature (up to 1569^{o}C), outlet air temperature (up to 1201^{o}C), and air pressure of up to 20 bars than the previous one in Karni. These results made the efficiency of this system increased up to 90% with unsymmetrical error bound +0.14/-0.08. The porcupine has very good performance as an absorber; it is potential to be used for a solar-gas turbine hybrid system, which needs high air temperature and pressure. The steady state condition of irradiation only occurred for 2 minutes; the other times the condition fluctuated. This condition also proved the stability of the porcupine receiver -in terms of thermal stresses. The receiver has very good thermal resistance because it was not damaged during the experiment.

An experiment conducted by Karni *et al.*[8] for the foam and honeycomb structure showed the importance of thermal conductivity properties of the material. Thermal conductivity is the material property required to transfer the heat through a unit thickness in a direction normal to a surface of unit area, due to a unit temperature gradient under steady state conditions[10]. It affects the ability of the receiver to reach a homogenous temperature while the light irradiation is not constant. If the absorber has high thermal conductivity, it can easily reach a homogenous temperature, thus preventing localized heating. In this

case, the foam and honeycomb structures had poor heat distribution due to low thermal conductivity and hence, localized melting and cracking occurred. High thermal conductivity also affects the mechanism of heat transfer during the process as stated by Fend *et al.*[11]. Compared to the alumina-silica honeycomb[8], the SiC[11] resulted in higher efficiency and higher outlet air-temperature for lower input irradiation (solar flux) while the honeycomb had localized melting. This is due to the low thermal conductivity of the alumina-silica materials.

A simulation of solar intensity distribution on the receiver conducted by Kribus *et al.*[12] showed that high thermal conductivity of the absorber caused the front surface temperature of the absorber become close to the back surface temperature thus increasing the radiation loss and lower the efficiency. Too low thermal conductivity will lead to local heating problem in the absorber. Therefore, it was concluded that the optimum value for the thermal conductivity is between 1-3 W/m.K.

High specific surface area is one of the important features for absorbers. It provides high transfer and a high absorption surface that lead to a high rate of heat transfer and low radiative losses by emissivity. Fend *et al.*[11] showed that the efficiency of the sandwich absorber is 10% higher than the non-sandwich absorber with 20 ppi (pores per inch). Sandwich material consists of two different foams, the front side is 80 ppi foam and the backside is 20 ppi foam. The large heat transfer surface causes the front surface cooled effectively such as the radiative losses were reduced. This experiment used an open-air system. They noticed that the high surface area in the front layer of absorber could increase the efficiency of the absorber by providing a large surface area for heat transfer; therefore, a higher cooling rate occurred there. The improved cooling rate will reduces

the radiative emission of the front absorber. Efficiency error was ±4.8 %. The efficiency was calculated from (power water + power air)/power of aperture. The system used water/air heat exchanger after the absorber and a fan to force the air flowing through the absorber.

Another experiment was conducted by Heller *et al.*[13]. They used a SiC foam with 20 ppi as the absorber material. It reached high outlet air temperature (up to 960^{o}C) with pressure of about 6.5 bars. Although they did not record the absorber temperature, the absorber temperature should be higher than 1000^{o}C. They showed the suitability of silicon carbide (SiC) as an absorber material without any damage occurring. The comparison table of those papers is shown in Table 1.

Gaining high flux from the sun increase input energy of the system. However, it increases the temperature of absorber. To gain high energy, the absorber should be able to withstand high temperature and should be both mechanically and chemically stable. It was clear that for such high temperature applications, metal materials would undergo significant deterioration in their strength although they have very high strength at room temperature. Therefore, ceramic materials are the best candidates for this application. It has relatively low strength compared to high strength metal, but it remains stable at high temperature. As shown by the previous studies, ceramic can withstand up to 1500^{o}C without any damage. However, the easiness of ceramic fracture should be considered during design because it can cause sudden failure during operation.

The other important properties are absorptivity and emissivity. The absorptivity (α) is the amount of radiation absorbed by a surface compared to the radiation absorbed by a black

body. This absorption will tend to increase the internal energy of the material hence increasing its temperature. The emissivity coefficient (ε) indicates the heat radiation of a 'grey body' based on the Stefan-Boltzmann Law compared with the heat radiation of an ideal 'black body' with ε = 1. This emissivity will be counted as energy loss from the material. Those properties are opposite each other. If the absorption increases, the temperature will increase. However, as temperature goes up, the emission of light will also go up. Therefore, some energy loss will occur. X. Xu *et al.*[1] reported that this radiation loss could reduce the thermal efficiency of the absorber from 92% to 72%. It showed that both of the properties, absorptivity and emissivity, should be optimized to increase the absorber efficiency.

The radiation loss lead some researcher used a special material, which can absorb most of the light but has low re-radiation properties. The idea is to absorb most of the high quantity wavelength comes from the sun and let the material has radiation loss from the low quantity wavelength as showed in the Figure 2 below. They called the material as selective absorber material.

As showed in the Figure 2, most of solar light that comes to the earth has spectral between 300 nm to 1800 nm. Therefore, the selective absorber will try to absorb the light in these ranges and emits the other range.

Table 1 Comparison of several references for ceramic absorber

Literature	Structure	Material	Solar Incident radiation (W/m^2)	Eff.	Max. Air Temp (^oC)	Max Absorber Temp (^oC)	Post-exp Condition	Air System	Efficiency
Leuchsner (1991)	Foam	Si_3N_4/ SiC coating	150-500	57%	960	-	Quartz window was cracked	Closed	Power efficiency : Qout/Qin (outlet temp, input radiation)
Karni, et al. (1998)	Porcupine	Al_2O_3-SiO_2	784-815	42-79%	940	1300-1400	No localized damage detected	Closed	Efficiency= Qout/Qin (mass flow rate, inlet temp, outlet temp, input radiation)
Karni, et al. (1998)	Foam	Al_2O_3-SiO_2	775	68%	547	1200	small cracks area appeared	Closed	Efficiency= Qout/Qin (mass flow rate, inlet temp, outlet temp, input radiation)
Karni, et al. (1998)	Honeycomb	Al_2O_3-SiO_2	821	56%	561	1300	Localized melting area appeared	Closed	Efficiency= Qout/Qin (mass flow rate, inlet temp, outlet temp, input radiation)
Kribus, et al. (2001)	Porcupine	Al_2O_3-SiO_2	895	70-90%	1201	1569	No damage detected	Closed	Efficiency= Qout/Qin (mass flow rate, inlet temp, outlet temp, input radiation)
Fend, et al. (2004)	Foam (one layer)	SSiC	863	76-94%	570	713	-	Open	Efficiency= (Power water+power air)/power on aperture
Fend, et al. (2004)	Foam (two layer)	SSiC	804	83-98%	618	800	-	Open	Efficiency= (Power water+power air)/power on aperture
Fend, et al (2004)	Honeycomb-like	SiC	500	80%	650	1200	-	Open	Efficiency= (Power water+power air)/power on aperture
Heller (2005)	Foam	SiC + SiO_2 Coating	900	70%	960	-	-	Closed	Efficiency= Qout/Qin (mass flow rate, inlet temp, outlet temp, input radiation)

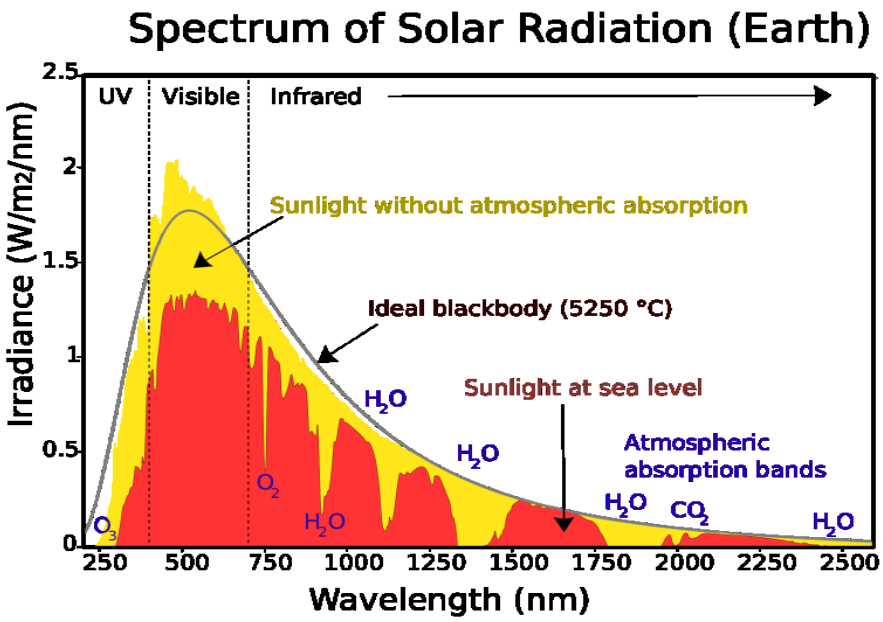

Figure 2 Radiation distribution of the sun at the earth surface (AM1.5 ("ASTM G173-03 Table", n.d.)) and typical black body radiation of an absorber at 673 K[2].

Sciti *et al.*[14] proposed new materials as solar absorber. They proposed hafnium diboride and zirconium diboride as the absorber because of its high absorbance over emittance ratio and better thermal properties compare to SiC. Sani *et al.*[15] also showed that zirconium carbide has lower radiation loss than SiC therefore it can be a good candidate for absorber material.

These optical properties may have huge effect to the overall efficiency of the system. Burlafinger *et al.*[16] studied this effect using simulation and come with conclusion that in all investigated cases, an operation temperature exceeding 1383 K shrinks the overall efficiency and the usable power output. It was shown that the highest reachable overall efficiency of a CSP plant for sun concentrations up to 2000 lies at 73% for a perfect

selective absorber and a maximum efficiency of around 65% is theoretically possible for a realistic selective absorber.

Fend *et al.*[11] stated that in all cases, to obtain high efficiencies, high absorptivity in the visible and near infrared range has to be combined with a high porosity to create large surfaces for convective heat transfer and light trapped mechanism inside the absorber. The visible and near infrared range absorption is important because most of the solar wavelengths that penetrate the earth's atmosphere are in these ranges.

The permeability of the absorber determines how the fluids flow inside the absorber. Fend *et al.*[11] said that higher permeability tend to reduce the possibilities of local heating inside the absorber hence increasing the efficiency of the heat transfer.

The previous researches showed that material properties have huge effect on the efficiency of the receiver. There are 5 (five) material properties which should be considered for selecting the absorber material. These are thermal conductivity, absorptivity, coefficient of thermal expansion, maximum operating temperature, and flexural strength.

Thermal conductivity plays a vital role in the heat transfer, energy conservation, and the durability of the material. Higher thermal conductivity will prevent local heating however, it can lower the temperature difference between front and back surface of the absorber. Thus, the radiation losses might happen in the front surface. This issue can be solved by having a good convection transfer that removes heat from the front surface faster than the heat transfer inside the absorber.

Absorptivity or emissivity should be considered because the higher absorptivity over emissivity ratio will lead to higher energy gain and lower radiation losses. The durability of absorber is also affected by the thermal expansion coefficient especially during fluctuated solar irradiation and on-off operation. The lower coefficient will prevent the possibility of ceramic to crack or fracture suddenly. The application of pressurized air in the system will cause some stress inside the material. Therefore, minimum flexural strength is important for the material.

Utilizing sun as the energy source has numerous drawbacks such as being available only in the daytime, inconstant irradiation throughout the day due to cloud movement and the whole year due to sun-earth relative position. These inconstant irradiations may cause thermal shock and thermal fatigue to the absorber. Hence, the thermal fatigue and thermal shock resistance properties should be considered to ensure the durability of the absorber.

Several ceramic properties of the absorber material are shown in Table 2 below. Considering their properties, the best candidate materials for this experiment are alumina, silicon carbide, and siliconized silicon carbide.

Table 2 Material properties of several ceramics

Material	**Flexural Strength (MPa)**	**Thermal Conductivity (W/m.K)**	**Coef. Thermal Exp. ($10^{-6}K^{-1}$)**	**Max. Operating Temp (^oC)**	**Melting Temp (^oC)**
Si_3N_4 (sintered)[10]	414-650	33	3.1	1600	1900
SiC (sintered) [10,17]	96-520	71	4.1	1650	2730
SiSiC [17,18]	300	130	5.5	1350	1420
Al_2O_3-SiO_2 [19]	158	5	5.5	1400	1900
Al_2O_3 [10,17]	282-551	39	7.4	1700	2050

2.1.2 Parabolic Dish

Manufacturing a parabolic dish from the scratch is very challenging because of its special shape, especially when the size is big and the small error in the curvature are needed. Those reasons are the requirement for the solar light reflector. Very nice surface and curvature of the parabolic surface is required to give the best quality reflected light hence the maximum efficiency can be achieved. The surface error estimation should be considered since the very beginning of the manufacturing process. Therefore, some calculations were done to estimate the minimum error that can be tolerated and achieved by the manufacturing system available in our workshop.

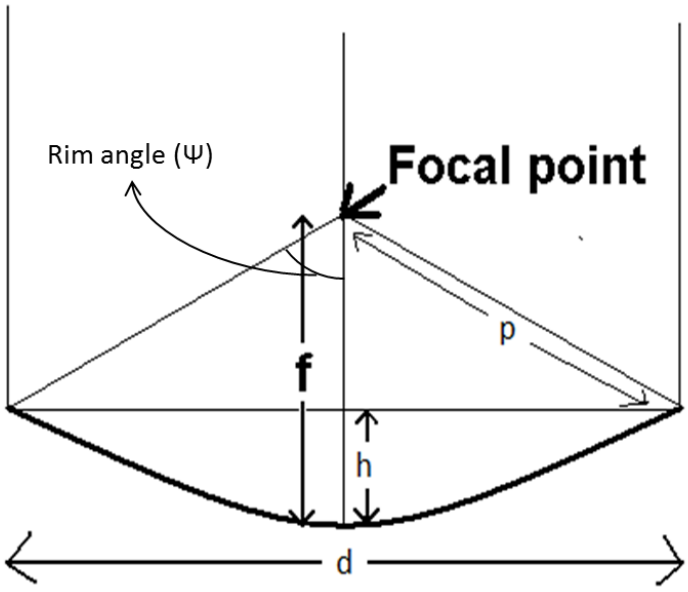

Figure 3 Schematic picture of several important parameters in parabolic shape

The dish diameter (d) is 5000 mm and the focal point (f) is 3000 mm. Using these known parameter, the height of the dish (h), the rim angle (Ψ), and distance from focal point to the edge of dish (p) can be calculated the following equations,

$$h = \frac{d^2}{16f}, \tag{1}$$

$$\tan \Psi_{rim} = \frac{1}{(d/8h)-(2h/d)}, \tag{2}$$

$$p = \frac{2f}{1+\cos \Psi_{rim}}, \tag{3}$$

These parameters are essential to estimate the size of focal plane of the dish (see Figure 3 for its schematic picture). The perfect surface dish will have one focal point however, it is almost impossible to achieve it theoretically and technically. Therefore, the focal plane is used to determine the area where all reflected light would be collected instead of a point. The focal plane of the dish is a circular shape. Theoretically, the minimum diameter (d_f) of focal plane possibly achieved (assumed perfect surface) would follow,

$$d_f = 2p \tan(\epsilon/2), \tag{4}$$

where ϵ = the finite angular size of the sun from the earth which is 9.6 mrad. The sun light never comes perfectly parallel to the dish and it has the width therefore the reflected light will be a distributed area rather than a point. The usual reported sun width is 9.6 mrad. However, because of forcing a standard distribution on the solar disc, the error of the sun (σ_{sun}) used is 2.8 mrad.

For our dish, theoretically the size of the focal plane is 33.8 mm. However, the equation will slightly different if the error of the dish were put into the consideration,

$$d_f = 2p \tan\left(n\left({}^{\sigma_{total}}/_{2}\right)\right), \quad (5)$$

While σ_{tot} is the total angular error contributed to the dish and n is the number of standard deviations being considered. The σ_{tot} are calculated using equation (6)[20],

$$\sigma_{tot} = \sqrt{(\sigma_{sun})^2 + (\sigma_{track})^2 + \left(\sigma_{slope}\right)^2 + \left(\sigma_{refl}\right)^2 + (\sigma_{abs})^2}, \quad (6)$$

Each of the components are,

σ_{sun} : sun rays not being perfectly parallel, therefore its width is considered

σ_{track} : concentrator alignment with sun

σ_{slope} : concentrator surface irregularities

σ_{refl} : mirror non-specular reflection

σ_{abs} : receiver alignment with focal point

The higher value of σ_{tot} (means higher error value) increase the focal plane radius of the reflected light, as shown in the Figure 4 below,

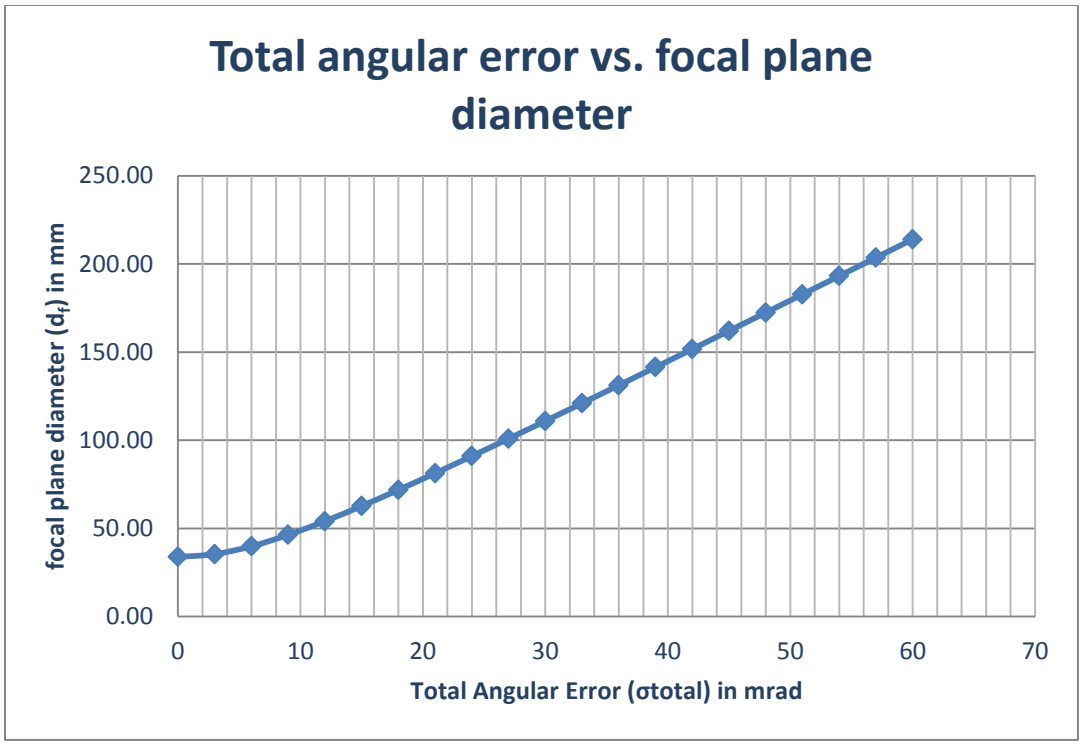

Figure 4 Graph that shows the relationship of total angular error and the focal plane diameter

As shown in the Figure 4, the higher distribution area of the reflected light reduces the maximum sun concentration ratio; hence, the energy harnessed per area will be lower.

As discussed in the following paragraphs, the usual process during analysis will use multiples of one standard distribution. Assume we define the σ_{sun}, σ_{track}, σ_{refl}, and σ_{abs} value. Then, let the σ_{track} error defined by 4 mrad, The σ_{refl} is 0.5 mrad, and The σ_{abs} is 2 mrad. Therefore, the relation between focal plane diameters versus slope error is showed in the Figure 5,

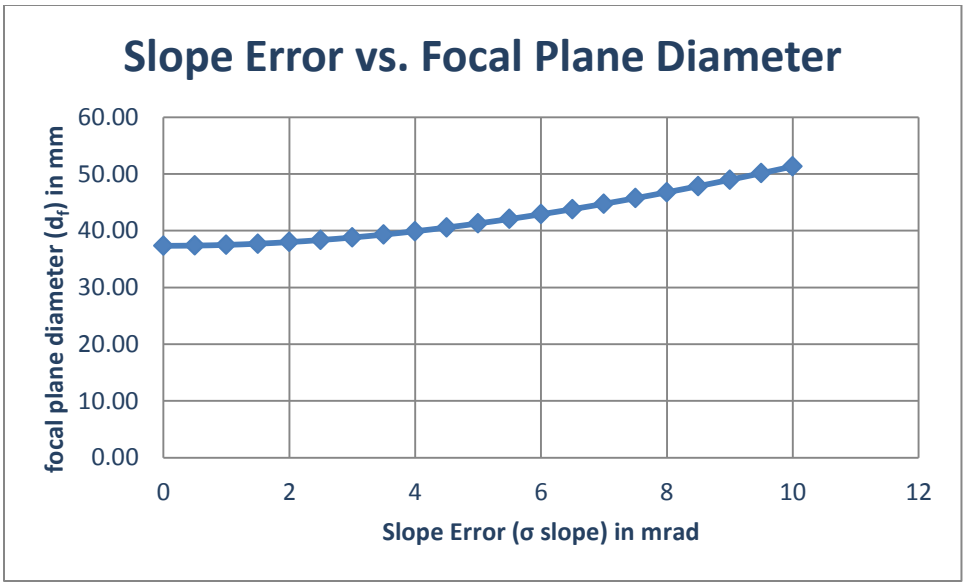

Figure 5 Graph that shows the relationship of slope error and the focal plane diameter

Values of σ_{slope} around 0.4 mrad are found in very accurate systems, although values up to around 5 mrad can be adequate, depending on the type of concentrator and its manufacturing method.

If we decide to have slope error (σ_{slope}) about 5 mrad and the other value we use the previous value mentioned, the total angular error of the dish are,

$$\sigma_{tot} = \sqrt{(2.8)^2 + (4)^2 + (5)^2 + (0.5)^2 + (2)^2} = 7.29$$

The flux capture fraction (Γ) that relates the percentage of light reflected to a desired circular area at the focal point with diameter (d_f) are,

$$\Gamma = 1 - 2 \times Q_x, \tag{7}$$

Where,

$$Q_x = f_x \times (b_1 \times t + b_2 \times t^2 + b_3 \times t^3 + b_4 \times t^4 + b_5 \times t^5), \tag{8}$$

$$f_x = \frac{1}{\sqrt{2\times\pi}} \times exp\left(-\frac{x^2}{2}\right), \quad (9)$$

$$t = \frac{1}{(1+r\times x)}\ , x = n/2, \quad (10)$$

$$n = \arctan\left(d \times \frac{\cos(\Psi_{rim})}{p}\right) \times (2/\sigma_{tot}), \quad (11)$$

and:

r = 0.2316419

b1 = 0.379381530

b2 = -0.356563782

b3 = 1.781477937

b4 = -1.821255978

b5 = 1.330274429

d = parabolic dish diameter, here = 5000 mm

Ψ_{rim} = Rim angle, here = 45.25^0

p = Distance from focal point to rim of the paraboloid, here = 3521 mm

therefore,

$n = \arctan\left(5000 \times (\cos(5.25)/3521)\right) \times (2/7.29) = 12.344,$

while $x = 12.344/2 = 6.172$

So,

$$t = \frac{1}{(1 + 0.2316 \times (12.344/2))} = 0.412$$

So,

$$f_x = \frac{1}{\sqrt{2 \times \pi}} \times exp\left(-\frac{6.172^2}{2}\right) = 2.133 \times 10^{-9}$$

So,

$$Q_x = 2.133 \times 10^{-9} \times (0.379381530 \times 0.412 + (-0.356563782) \times 0.412^2 + 1.781477937 \times 0.412^3 + (-1.821255978) \times 0.412^4 + 1.330274429 \times 0.412^5)$$

$$Q_x = 2.133 \times 10^{-9} \times 0.1836 = 3.92 \times 10^{-10}$$

Therefore the flux capture fraction (Γ) is,

$$\Gamma = 1 - 2 \times 3.92 \times 10^{-10} = 0.99$$

It means the 5 m dish with slope error 5 mrad captures 0.99 fraction of the sun light that comes through the aperture. Then it will be reflected to the receiver. This value is more than enough to prevent the reflected loss of the light capture.

One can expect 68 percent of the energy incident on that part of the reflecting surface (defined by *p*) to fall on line d_f when *n* is chosen to be equal to 2 (i.e.±1 σ_{tot}). It is common to use ± 2 to ± 3 times in solar analyses to ensure that 95 percent or more of all possible energy is captured.

Table 3 Percent of Measurements of Flux Falling Within Multiples of a Given Standard Deviation (σ)

Multiples of Standard		Percent
Deviation (σ)	n	Within Limits
±I	2	68.27 %
±2	4	95.45 %
±3	6	99.73 %

If we use normal distribution (Table 3);

with n = 2, 68% of the light fraction will be inside 51 mm circular focal plane

with n = 4, 95.5% of the light fraction will be inside 103 mm circular focal plane

with n = 6, 99.7% of the light fraction will be inside 154 mm circular focal plane

2.1.3 Heat and Flow-rate Requirement

In the parabolic dish application, the fluid that flows through the absorber had significant change in their properties during the heat transfer. Because the temperature different is very high between the inlet temperature (273 K) and outlet temperature (1073 - 1273 K). Because of its high operating temperature, the design of experiment decided to air as the heat transfer fluid. The flow properties of the fluid also affect the heat transfer efficiency between the absorber and the fluid. One of the important parameter is the flow rate. Based on the general heat energy equation,

$$Q = \dot{m} \times C_p \times \Delta T, \tag{12}$$

the flow rate could be estimated for the total energy available. In our work, the maximum power of the dish is about 20 kW. If we assume the inlet air temperature is 300 K, while the estimated minimum outlet air temperature is 850 K and the maximum is 1150 K. The heat capacities of air (Cp) are 1.040 kJ/kg.K and 1.110 kJ/kg.K at 550 K and 850 K respectively [21]. The density of air at 300 K is 1.1614 kg/m^3. The flowrate of the air inside absorber are,

- Minimum flowrate:

  Minimum $\dot{m} = \frac{Q}{\overline{C_p}(T_o - T_i)} = \frac{20\ kW}{1.110\ \frac{kJ}{Kg.K}(1150\ K - 300\ K)} = 0.01609\ Kg/s$

  Minimum volume flowrate:

  $$\forall = \frac{\dot{m}}{\rho} = \frac{0.01609\ \frac{Kg}{s}}{1.1614\ \frac{Kg}{m3}} = 0.01385\ \frac{m3}{s} = 13.85\ L/s$$

- Maximum flowrate:

  Maximum $\dot{m} = \frac{Q}{\overline{C_p}(T_o - T_i)} = \frac{20\ kW}{1.040\ \frac{kJ}{Kg.K}(850\ K - 300\ K)} = 0.03846\ Kg/s$

  Maximum volume flowrate:

  $$\forall = \frac{\dot{m}}{\rho} = \frac{0.03846\ \frac{Kg}{s}}{1.1614\ \frac{Kg}{m3}} = 0.03312\ \frac{m3}{s} = 33.12\ L/s$$

These maximum and minimum values of flowrate will help the selection of blower or pumping machine, which will be installed in the system.

2.1.4 Receiver Design

Receiver is an important part where the heat transfer between the solar light, absorber, and fluid, takes place. The receiver design depends on several factors, such as the fluid used, absorber specification, open or closed system, and the light reflector design. The material of the receiver parts also important to ensure the longevity and good efficiency of the receiver itself. Since we build up our own system from the scratch, we went through several designs, back and forth. Not only the functional factor but also the economic factors were put to our design consideration to make the relatively cheap, tough, and good performance receiver.

The reflector or collector design will determine the shape of reflected light; hence, it will govern the suitable shape of the receiver and the absorber. For example, the parabolic trough have line shape reflection, hence the receiver and absorber is in the tubular shape. In parabolic dish, the reflection is circular shape. Therefore, the receiver and absorber design will have circular-based shape.

The absorber specification such as the shape (volumetric, 2D, particle size, etc), the material (metallic or ceramic), and surface area structure (solid, foam, or composite structure) will determine how the flow of the fluids going through the absorber. The flow direction will govern the receiver shape to make sure it connects efficiently to the reflection of the light. This factor also includes how receiver provides the mechanism to change/replace the absorber in case it broken or damaged.

The closed system means the fluid comes from certain inlet which has specific controlled parameter, while open system means the fluid comes from ambient/atmospheric

condition. The closed system needs isolated chamber, which separated from ambient environment. Hence, it will have more complicated structure, especially if the fluid is pressurized with high pressure.

The type of fluids will determine the material of the receiver parts. The better material compatibility between working fluid and the receiver part will increase the chemical stability of the receiver hence its lifetime will be increased.

All of those factors should be considered together with the economical factor and manufacturing ability of the workshop. Therefore, the receiver with optimized properties could be made properly.

We decided to use air as heat transfer fluids, circular foam absorber, and closed system. Therefore, we made the receiver shape like a tube with two different chambers made from stainless steel, a quartz window, and a ceramic sleeve as insulator.

2.1.5 Thermal Conductivity

Thermal conductivity of the absorber plays vital role in the heat transfer process and the integrity of the material. Since the absorber is in the foam structure, its intrinsic thermal conductivity has changed significantly due to low proportion of solid material and the air presence between the solid structures. It will definitely lower as the portion of the porosity increased. It called effective thermal conductivity (ETC). Many of researchers are trying to estimate the effective thermal conductivity through modeling or experiment.

Several experiments were conducted to measure the real effective thermal conductivity. People are using different experimental method to estimate and measure this property, some of them even trying to make more complicated model that can predicted effective thermal conductivity of open celled ceramic foams.

There are two most used methodologies to measure effective thermal conductivity of foam specimen, which are steady-state and transient methods. The steady-state methods available in the literature are generally based on either guarded hot-plate, which based on standard ASTM C 177 (see Figure 6). A guarded hot-plate apparatus is normally used to determine the two-phase thermal conductivity. The setup use reference methods to determine the two-phase thermal conductivity of the sponge samples. All these techniques share the fact that exact knowledge of the heat flux through the sponge sample is necessary. The usage of the reference method exhibits advantages due to the homogeneity of the reference sample, which is the same in diameter as the sponge sample. Dietrich *et al.*[22] measured ETC of alumina, mullite, and CBSiC foams, with various pore densities and porosities in the range from 75% to 85%. Their results were obtained for moderate temperatures 100^{o}C using a guarded hot-plate apparatus in combination with a numerical procedure in order to correct the heat losses. Dietrich *et al.* showed that their model was good enough to predict their experimental results with error about 2% for alumina. The results of effective thermal conductivity are about 1.8 - 2 W/m.K for alumina 85% porosity and 20 ppi. However, for another sample (alumina and mullite) gave high error, which is more than 20%.

In this method, the contact between sample and the hot plate will determine the homogeneity of heat flux, which is coming to the sample. Some people prepare the

sample by grinding to ensure the flatness of the surface, while the standard (ASTM C 177) propose to use some thin sheet of rubber and applying some forces.

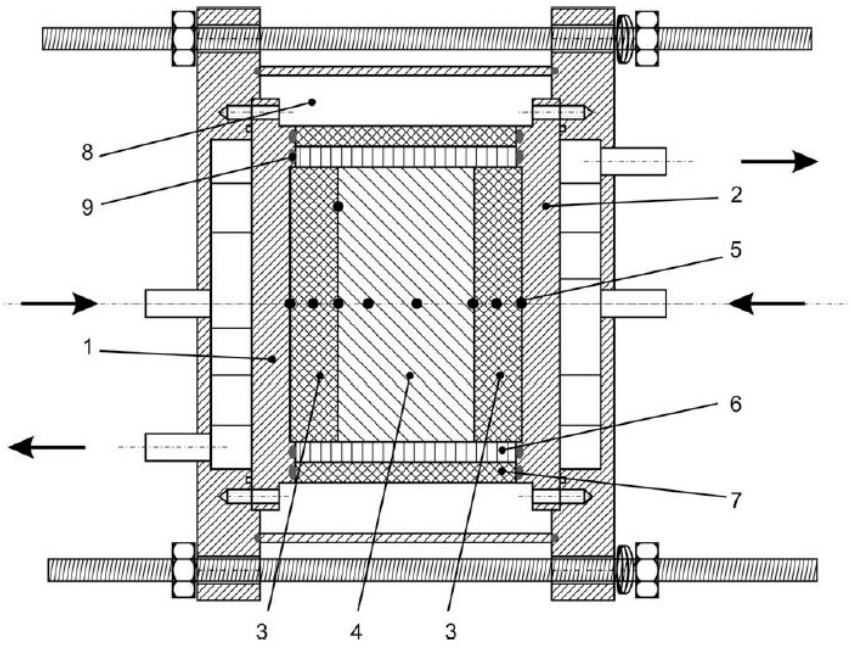

Figure 6 Experimental setup for the determination of the two-phase thermal conductivity: (1) heating plate, (2) cooling plate, (3) Teflon cylinder, (4) sponge, (5) thermocouples, (6) polystyrene insulation, (7) Teflon insulation, (8) vacuum chamber, and (9) o-rings.[22]

Another popular method is transient methods for measuring ETC of ceramic porous foams. In this method, an insulated sensor is placed between two identical parallelepipedic foam samples that simultaneously serves as heat source and resistance thermometer, as shown in Figure 7. After applying a constant current to the heating element of the sensor, a transient, ellipsoidal temperature field developed. By correlating the resulting time evolution of the temperature with the thermo-physical properties of the foam samples, ETC is determined. The sensor is sandwiched between the two foam samples, their surfaces are polished in order to improve the contact between sample and sensor.

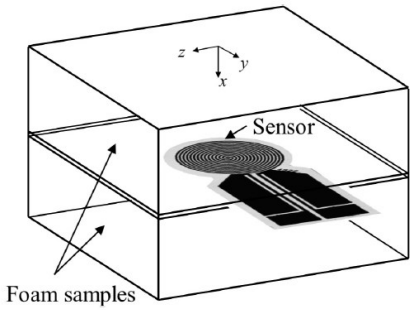

Figure 7 Schematic representation of foam samples and sensor assembly for transient plane source technique.[23]

Mendes *et al.*[23] showed that they could produce very good agreement between model and the experiment results. The ETC for 10 ppi Al_2O_3 was about 1 – 1.5 W/m.K below 200oC. This supports the argument that TPS technique measures a directionally averaged ETC. After appropriate validation, which would require several case studies involving porous foams of different materials, pore densities and sizes, this approach could provide a viable experimental procedure based on TPS technique that would allow the measurement of true directional ETC of anisotropic foams.

Regarding the surface contact between the sample and the sensor, they prepared the foam by grinding to provide smooth and flat surface. It increase the surface contact between sample and the sensor, therefore the heat could be transfer more efficient.

There is one recent method to measure thermal conductivity, which is called Modified Transient Plane Source (see Figure 8). It use almost similar heating element and working principle as TPS, however it needs only one surface contact between the element and the sample. It can measure a lot of different materials in terms of the physical shape, such liquid, foam, powder, and solid.

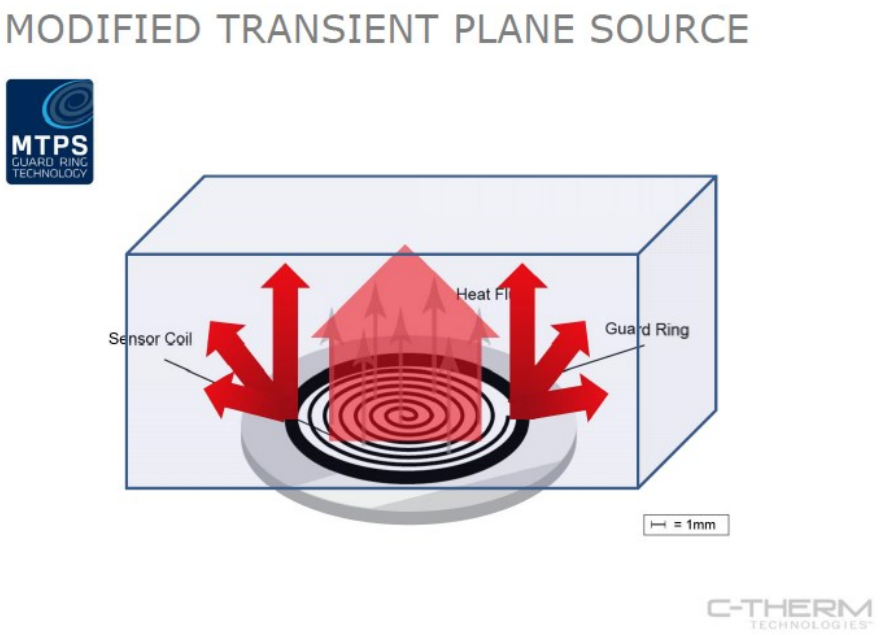

Figure 8 Schematic representation of foam samples and sensor assembly for modified transient plane source technique [24].

2.2 Statement of the Problem

Based on the previous studies and literature, no studies are available that have studied the effect of absorber material properties on the performance of the receiver in a controlled systematic experimental program. Since the absorber properties are very important, such experiment to compare different materials in the same condition must be done. Therefore, we can discover how extent the relation between those material properties and how much they affect the performance of the receiver.

The huge potential of solar energy in KSA region and the absence of local solar dish manufacturer encourage us to find out the possibility to manufacture the system (Dish, receiver, and absorber) inside the kingdom. Therefore, the utilization of the system inside the kingdom becomes more reliable and cheaper.

2.3 Thesis Objectives

Based on the stated problem mentioned, we would like to fill the gap in the research. Hence, our intent is to compare different materials and explain to what extent material properties affect the performance of the receiver in the same experiment. Therefore, the objectives are:

a. Prepare an experimental setup to measure the effects of different material properties on the thermal performance of porous absorbers for solar turbine application at different conditions, which includes;
   - Design and manufacture a receiver
   - Design an experimental setup
   - Design the experiment matrix and material selection

b. Evaluate materials resistance and integrity through thermal fatigue experiment, which includes;
   - Thermal fatigue experiment
   - Stereomicroscope imaging
   - Effective thermal conductivity measurement
   - XRD analysis
   - SEM and EDS analysis

2.4 Scope of the Thesis

The thesis elaborates its content in the several parts, which are;

a. The first part is the introduction to the field.
b. The second part explains the literature review of the focus subject, which is absorber, basic theory, and the objectives of the thesis.
c. The third part describes the preparation made to support the parabolic dish manufacturing, experimental method, and measurement conducted in the thesis.
d. The fourth part shows the results of experiments, measurements, and characterizations of the absorber and the discussion related to the results.
e. The fifth part is the last part, which will conclude the work results and the recommendation for future research.

CHAPTER 3

METHODOLOGY

The research presented consists of design and experimental work. The design scope is preparing the experimental setup for solar thermal power plant, while the experimental scope is performing thermal cycle simulation of absorber specimen.

3.1 Design Work

The design includes helping the manufacturing of the dish, the absorber and receiver design consideration, and solar exposure experimental design of the whole system.

3.1.1 Dish

The dish was manufactured at KFUPM Mechanical Engineering Workshop in building 1. The undergraduate students manufactured the dish from the beginning. They designed and manufactured the mold, mold frame, material, and the structure that will support the dish on the ground. Assistance was given to help them during molding process, determining the surface accuracy and its effect on the dish performance. The diameter decided for the dish was 5.0 m with a focal point 3.0 m. The dimensions were chosen based on optimum size in terms of cost and energy consideration. The dish theoretically provide about 20 kW of solar energy (assumption solar irradiation is 1 kW/m^2).

3.1.2 Absorber

The Absorber is the main part inside the receiver that transfers the heat from the reflected solar radiation to the fluid. As mentioned before, ceramic material will be used for the absorber. The absorber specifications that should be considered in the design include the shape, structure, dimension, and the material. The absorber is in the circular shape with specific diameter and thickness matching the focal plane shape of the dish. In terms of the structure, we chose the foam ceramic structure with circular shape (Figure 9). It is widely used in the similar application and relatively easy to be applied in the receiver design. The absorber was purchased from a supplier, Fraunhofer IKTS Germany. The decision to purchase the sample was caused by the manufacturing complexity of the foam structure, which cannot be manufactured in the KFUPM lab.

Figure 9 Circular foam absorber used in the main experiment; SiSiC, SiC, and Al_2O_3 (from left to right)

The target temperature is 1000^{o}C or 1273 K; the ideal concentration (neglecting conduction and convection) was calculated based on the equation below [25]. It is shown in the Figure 10 that the ratio needed is, at least, 300 sun ratio. However, if the conduction, convection, and error of the dish specification are considered, it is better to get a higher

sun ratio for compensation. Based on the other graphs in Figure 11, to get a possible efficiency of 70% at 1200 K, the concentration needed is 1000. With a dish of 5 meters, the maximum absorber diameter should be 154 mm.

$$T_{abs} = T_s\left[(1-\eta) \times \left(\eta_{opt}/\in_{abs}\right) \times CR \times \sin\theta^2\right]^{1/4} \tag{13}$$

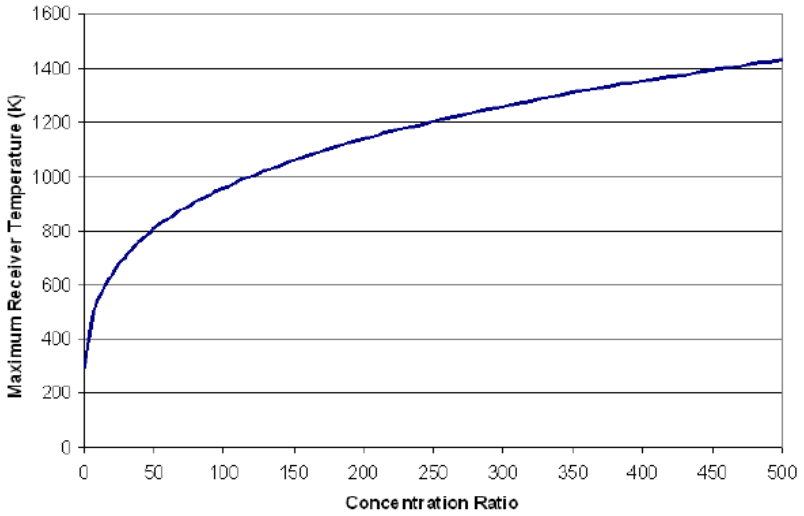

Figure 10 Receiver temperature vs. concentration ratio.[25]

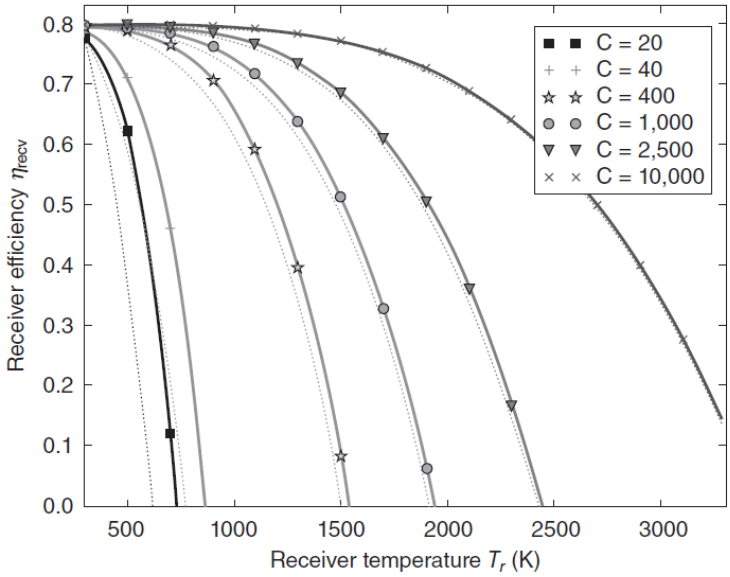

Figure 11 Efficiency of a simplified solar collector with 100% optical efficiency, average absorptivity of 0.8 (assumed equal to emissivity). DNI is 800 W/m^2, ambient temperature 300 K, and sky temperature 270 K.[26]

Determination of the absorber size not only depends on the concentration ratio, but also the dish dimension and error specification. Dish specification will determine the focal plane diameter in the receiver. If the dish is perfect, the minimum diameter of focal plane for a 5 m diameter dish is 33.8 mm. Therefore, the absorber diameter decided was 100 mm (between 33.8 mm and 154 mm) after considering surface slope error of the dish and the normal distribution of solar radiation on the focal plane which is 95.5% of the reflected light would be inside 103 mm of focal plane. The thickness of the foam is 10 mm, 20 mm, and 30 mm based on the thicknesses used in references.

Three different materials (alumina, silicon carbide, siliconized-silicon carbide) will be used for the absorber in this experiment. Those are the widely used material for this application. The supplier also provides 3 (three) small samples for initial characterization which has cuboid shape with dimension 35 x 35 x 20 mm. These samples were used for thermal fatigue experiment, measuring thermal conductivity, analyzing phase composition (EDS and XRD), and observing microstructure (SEM) of the foam.

3.1.3 Receiver

Receiver is a system that consists of absorber, the window glass, o-ring, air, insulation, and the supporting structure. It should be isolated from the environment. Therefore, it must have very good thermal insulation to prevent the heat loss. The main structure of the receiver was made of metal (stainless steel and aluminum) while other parts such as the absorber, window glass, and insulation part is made of mullite (Aluminosilicate).

The shape of the receiver depends on the absorber and solar collector system. Solar collector system used here is a parabolic dish mirror producing circular shape of the reflected sunlight. We decided to use ceramic foam structure as an absorber. The simple way to accommodate those two-design considerations is a cylindrical receiver with two main chambers.

The combining method of these parts is very important because the system experience fluctuating conditions at high temperature that cause different thermal expansion throughout the receiver. The designing and manufacturing phase consider the absorber specification, thermal expansion properties of each part, and literature review of similar application to build the optimum receiver. The thermal expansion coefficient used for mullite (as insulator) is 5.3×10^{-6} /^{o}C and stainless steel 304 (as main cylinder) is 18.7×10^{-6} /^{o}C.

The receiver was manufactured and assembled at KFUPM Mechanical Engineering workshop. It was made from standard stainless pipe, aluminum, and ceramic for insulation. The cutting, machining, and welding of the part were done in the workshop. Except the glass window and the insulator, which were manufactured outside the Kingdom. The window will use a special glass (fused silica), which can sustain about 200 degree Celsius without crack and transmit IR spectrum to ensure measurement with IR camera for the absorber during experiment.

3.2 Experimental Work

3.2.1 Sample specification

In our experiment, we used ceramic foams in cuboid shape (Figure 12) with 20 mm in thickness and ranging between 15-29 mm in both width and length. The difficulties during cutting process made the dimension were difficult to control. The foams made of aluminum oxide (Al_2O_3), silicon carbide (SiC), and siliconized silicon carbide (SiSiC) supplied by IKTS Fraunhofer, Germany. SiSiC consist of free silicon metal and silicon carbide with composition of 30:70, respectively. The physical properties of the foam are provided in Table 4.

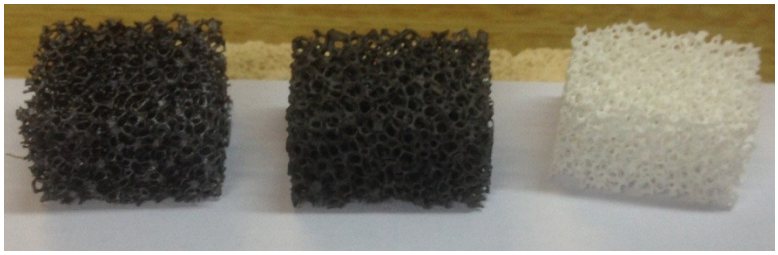

Figure 12 The cuboid foam ceramic used in the thermal fatigue experiment

The foams have 20 ppi (pores per inch) and 85% porosity. It means the foam has roughly about 20 pores per inch with cell size approximately 0.043 inch (1.08 mm) in diameter. The bulk-sample surface area to volume ratio of the cuboid foam and the circular foam (for main experiment) were 0.27 and 0.21 respectively. The thickness of cuboid foam is approximately 20 mm and the surface area to volume ratio of the cuboid foam about 1300-1470, thus the cuboid foam is representative enough for the circular foam.

Table 4 Several physical properties given by the supplier.

Properties	**Symbol**	**Unit**	**SSiC**	**SiSiC**	**Al_2O_3**
Purity	-	%	99.5	99	98
Porosity	-	%	85	85	85
Cell size	-	ppi	20	20	20
Compressive strength	σ	MPa	0.9	2.7	1.6
Specific surface area	S_v	m^2/m^3	1470	1390	1300
coefficient of permeability	K	m^2	$5.06x10^{-8}$	$6.72x10^{-8}$	$2.74x10^{-8}$
Inertial coefficient	β	1/m	480	523	861
Theoritical material density	ρ_{theo}	g/cm^3	3.15	2.83	3.9
Foam density	ρ_{foam}	g/cm^3	0.36	0.45	0.56
Strut density	ρ_{strut}	g/cm^3	2.14	2.83	2.34
Thermal conductivity	λ	W/mK	0.5632	-	-
Maximum operation temperature in air	T_{max}	^oC	1600	1350	1700

3.2.2 Measurement and Characterization

There are several measurements and characterizations conducted to provide good results and analysis.

a. Thermal conductivity

We measured the effective thermal conductivity (ETC) at room temperature using the Modified Transient Plane Source (MTPS) according to ASTM D7984 – 16. In this method, an insulated sensor was placed below the foam, providing one-directional heat flow and acting as resistance thermometer (Figure 13). Water as a contact agent was applied to ensure good surface contact between the foam and heating element. MTPS method with C-Therm TCi® was used to measure the thermal conductivity of the sample before the experiment and after 200 cycles. This equipment (C-Therm TCi®) gives direct value of thermal conductivity.

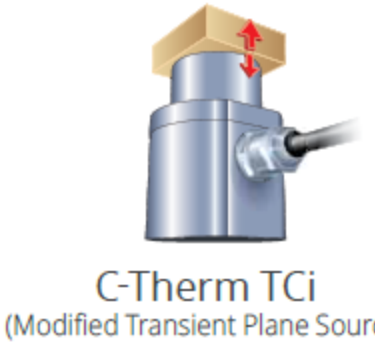

Figure 13 C-Therm TCi probe with sample on the top [24].

The procedures of measurement are,

- **Step 1 – Prepare the materials to be tested.**
- **Step 2 – Apply the contact agent**
- **Step 3 – Position the material on the sensor.**
- **Step 4 - Click the New Test button, select the project, select the test method to be used.**

  A test method describes the parameters of a test: when to take measurements, what power level and timing parameters to use, and how many measurements to take. Select a test method that uses a calibration method with the calibration material group and power level appropriate to the test material.
- **Step 5 – Select the Material Group, material to test, select the instrument, select the sensors, select the contact agent.**
- **Step 6 – Click the Start Test button.**

  The test results table is displayed. The test can be paused or stopped by clicking the appropriate button at the top of the test window. The samples are displayed as they are taken.

The overall accuracy of the TCi is estimated at 5% between 0°C and 50°C, and up to 10% above or below that temperature range. The variation is typically 1-2% (%RSD calculated from at least 10 consecutive samples, at 0°C to 50°C).

b. Stereomicroscope Imaging

We used stereomicroscope to observe the macro-crack that occurred in the sample. The magnification of the microscope is good enough to see crack length within good coverage area of the foam. We used minimum magnification which is 7.5x and 10x. As-received image were captured before thermal fatigue experiment. The stereomicroscope observation was conducted after certain cycles to monitor the crack initiation and propagation.

c. XRD and EDS

The elemental composition analysis of the foam, before and after the experiment, was conducted using EDS. X-Ray Diffraction examination was performed as compliment for the EDS results. The angle (theta) used in XRD were between 5^{o} – 90^{o} which wide enough to cover most of the phases pattern. The result of XRD is patterns that determine the chemical composition and crystal structure of the sample. These analyses provide examination of absorber whether they have phase transformation or not during thermal fatigue experiment.

d. SEM

SEM was used to observe microstructure of the foam and the surface morphology of the strut. Numerous magnifications from 25x up to 1000x were performed to provide clear images of the foam, before and after the thermal fatigue experiment.

3.2.3 Experimental Setup

a. Thermal Fatigue Experiment

In the thermal fatigue experiment, the samples (ceramics foam) were heated in a furnace to a given temperature then removed from the furnace and rapidly cooled to room temperature using forced convection. This is considered one cycle. The parameter and procedure of the experiment explained below.

- Parameter

- Two different temperature: 800^{o}C (1073 K) and 1000^{o}C (1273 K).
- Minimum temperature: room temperature, 25^{o}C (298 K).
- Heating rate: as fast as furnace can do.
- Holding time: 15 min.
- Cooling method: air forced convection using a fan.
- Number of cycles: begin from 1, 4, 16, up to 200 cycles.

- Procedure

a. Turn on furnace and start heating the furnace.
b. While it reaches the maximum temperature, put on all 3 sample in the furnace on the top of ceramic tray.
c. Close the furnace and the holding time start.
d. Open furnace at maximum temperature and take out all sample.
e. Cool samples to room temperature (1 cycle).
f. Check under microscope; observe the macro-crack.

g. Repeat step a-f for every cycle.

h. When reaching 200 cycles, stop the experiment. Characterize the sample using SEM, EDS, and XRD.

- Matrix

Table 5 Matrix of the experiment

Material	Maximum Temp. (K)	Label code	Cycles									
			1	4	16	25	37	65	82	123	185	200
SiC	1073	SiC1073	✓	✓	✓	✓	✓	✓	✓	✓	✓	✓
SiSiC	1073	SiSiC1073	✓	✓	✓	✓	✓	✓	✓	✓	✓	✓
Al_2O_3	1073	AlO1073	✓	✓	✓	✓	✓	✓	✓	✓	✓	*F
SiC	1273	SiC1273	✓	✓	✓	✓	✓	✓	✓	✓	✓	✓
SiSiC	1273	SiSiC1273	✓	✓	✓	✓	✓	✓	✓	✓	✓	✓
Al_2O_3	1273	AlO1273	✓	✓	✓	✓	✓	F				

F : Failed due to macrocrack
*F : Failed due to microcrack

- Thermal cycle experiment design

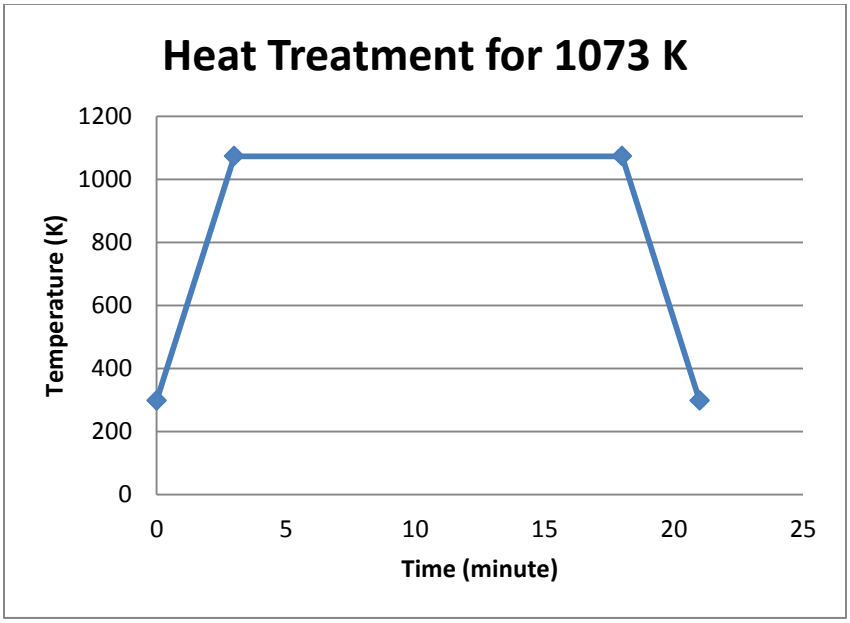

Figure 14 Heat treatment profile for temperature 1073 K

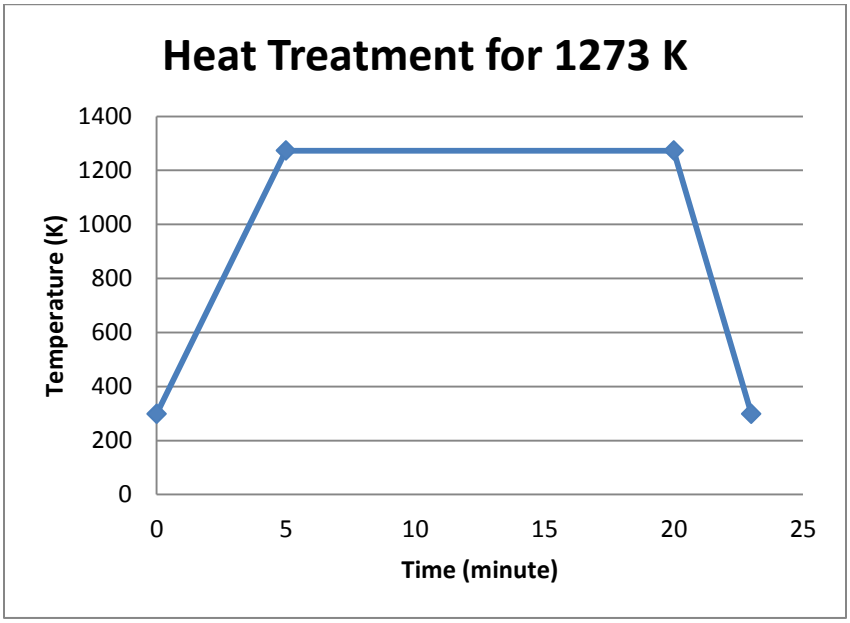

Figure 15 Heat treatment profile for temperature 1273 K

CHAPTER 4

RESULTS AND DISCUSSION

This chapter will cover the experimental results and its discussion. The sub-chapter divided based on the data specification and started by presenting the results then followed by the discussion.

4.1 Receiver Design

We succeeded manufacturing a receiver based on the previous design considerations (Section 2.1 and 3.1). The picture of assembled receiver and its schematic are showed in Figure 16. The complete technical drawings of all receiver parts are provided in the Appendix C.

An experimental setup for further experiment is proposed in this section. Figure 17 shows the complete design setup that includes the dish, receiver, IR-camera, pyranometer, flowmeter, thermocouple, and data acquisition systems (DAS) arrangement.

(a)

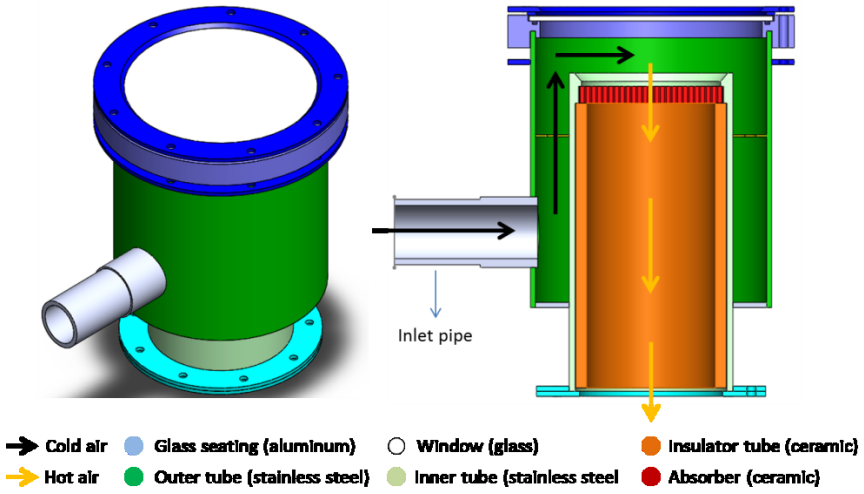

(b)

Figure 16 Receiver drawing in (a) a photograph and (b) schematics, where the left picture is the isometric view and the right picture is cross-section view.

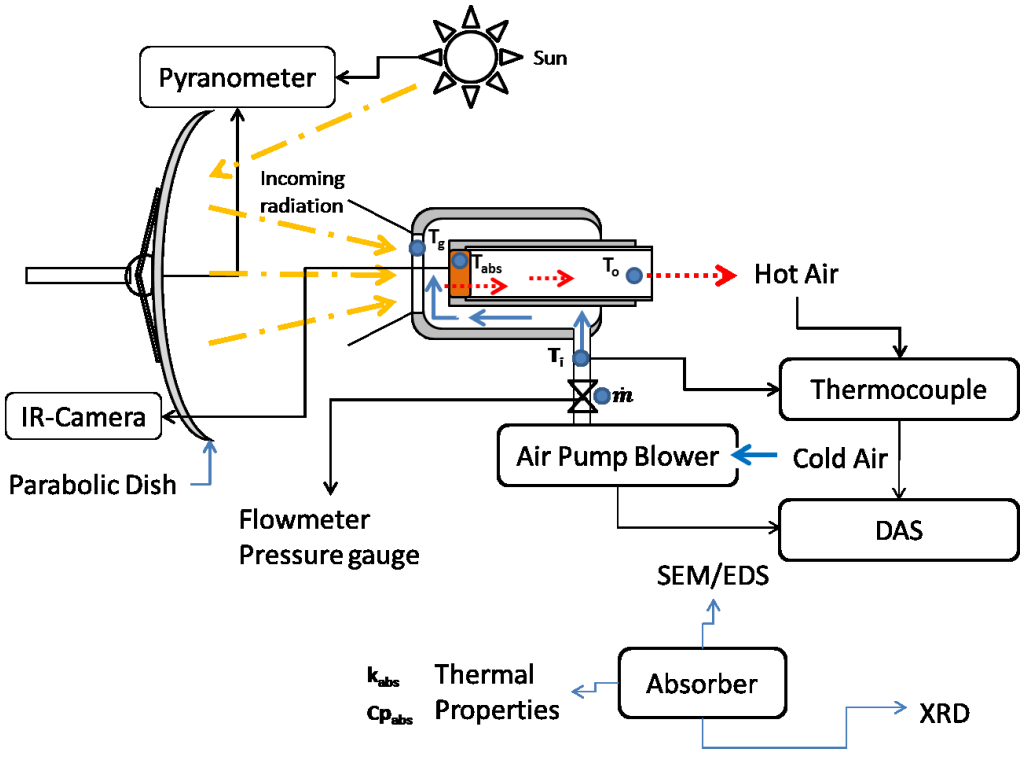

Figure 17 Schematic picture of the proposed setup of the main experiment

4.2 Effective Thermal Conductivity

Figure 18 and Table 6 show the ETC of as-received sample and after thermal fatigue experiment at 1073 K and 1273 K measured at room temperature.

Table 6 ETC measured at room temperature after 200 cycles at 1073 K and 1273 K

Sample	Effective Thermal Conductivity (W/m.K)		
	As-received	1073 K	1273 K
SiC	1.082 ± 0.006	0.973 ± 0.026	1.086 ± 0.079
SiSiC	1.172 ± 0.015	1.164 ± 0.038	1.316 ± 0.044
Al_2O_3	0.926 ± 0.009	0.905 ± 0.086	0.990 ± 0.096

The results indicate no significant change in the measured ETC. In the microscopic image and phase analysis shown in Section 4.4 and 4,5, we notice that no phase transformation occurred. The chemical stability of samples agreed with the result of thermal conductivity. We conclude that ETC of the sample at room temperature was not affected by the thermal fatigue experiment performed at 1073 K and 1273 K.

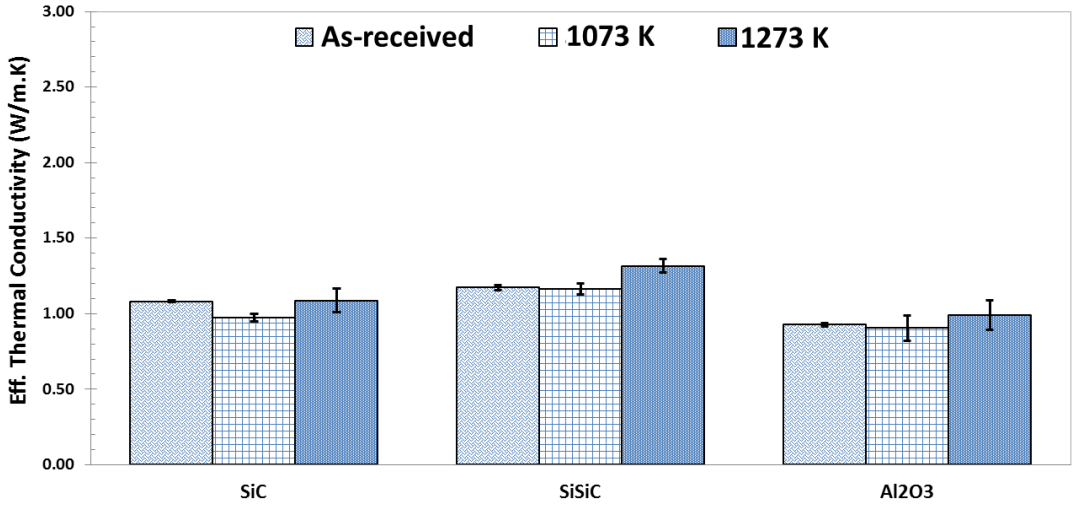

Figure 18 Effective thermal conductivity measured at room temperature after 200 cycles at 1073 K and 1273 K

4.3 Macroscopic Evaluation of Crack

This section discussed the crack evaluation. As mentioned in chapter 3, we used stereomicroscope to observe the crack appeared in the sample. The sample is cuboid that has 6 sides. The schematic picture of the side where the image taken is presented in the Figure 19.

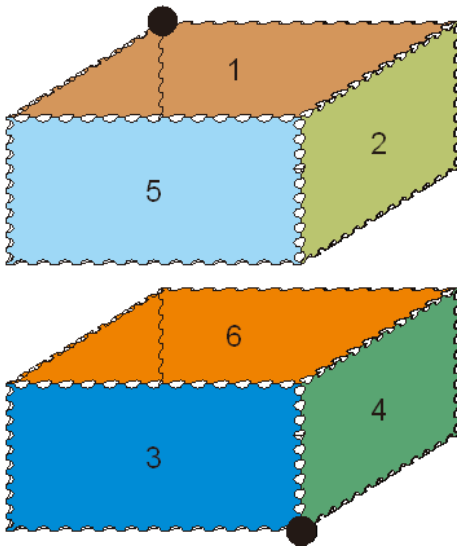

Figure 19 Schematic of side reference numbering.

The stereomicroscope images of the samples, before and after 200 cycles of the thermal fatigue experiment, were taken at the same area. In Figure 20 to Figure 23, SiC and SiSiC foams showed no macro-crack after 200 cycles of thermal fatigue experiment at 1073 K and 1273 K. No significant change detected in their images. SiC and SiSiC ceramics are very hard materials, have lower coefficient of thermal expansion than the Al_2O_3 (provided in Table 2) and have better thermal shock resistance as shown in Figure 24. These are reasons both of them can withstand 200 cycles at 1273 K without cracking.

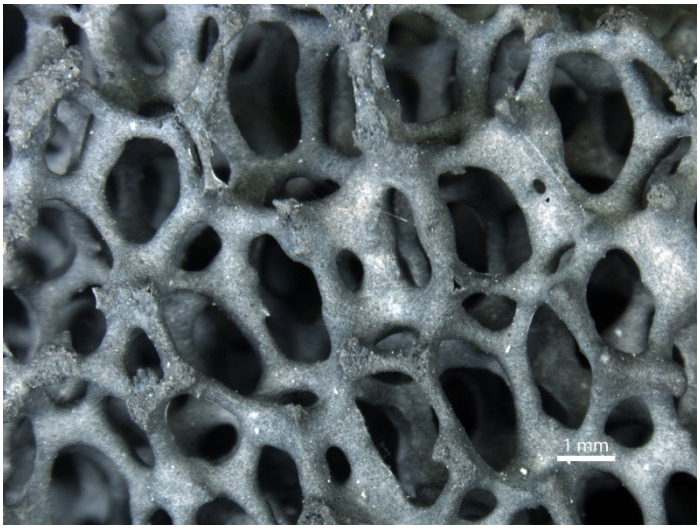

(a)

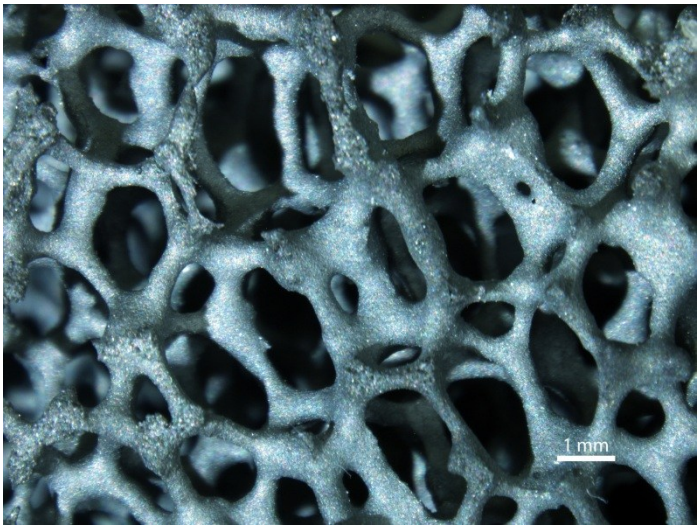

(b)

Figure 20 Stereomicroscope images of SiC (a) before and (b) after 200 thermal cycles at 1073 K (7.5x magnification)

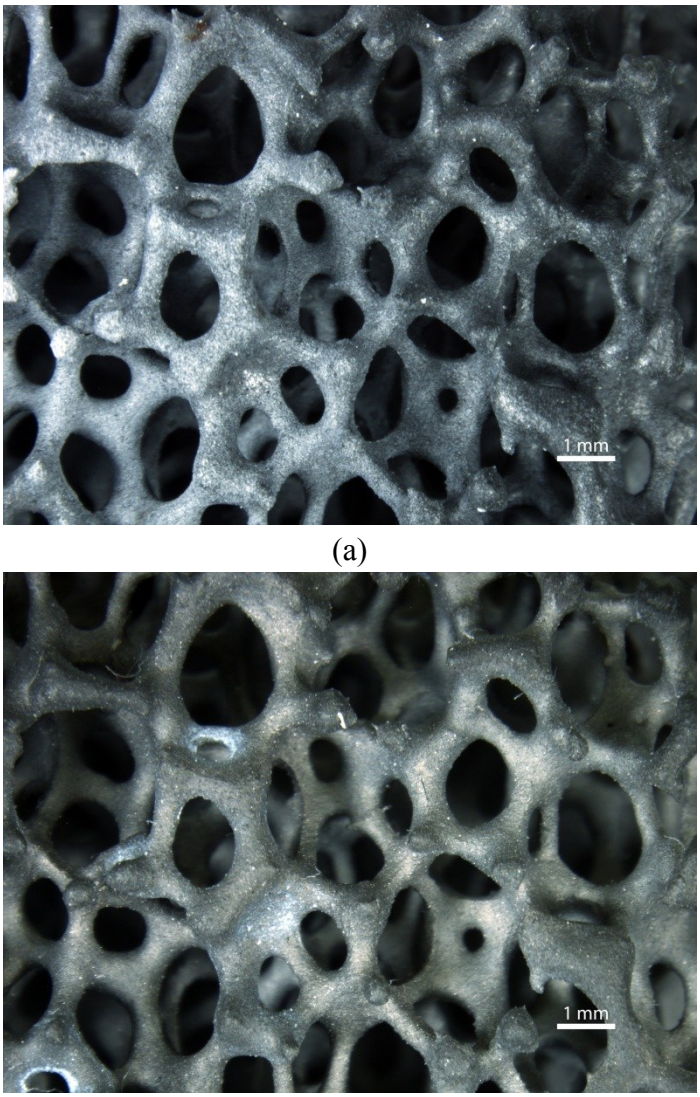

(a)

(b)

Figure 21 Stereomicroscope images of SiC (a) before and (b) after 200 thermal cycles at 1273 K (7.5x magnification)

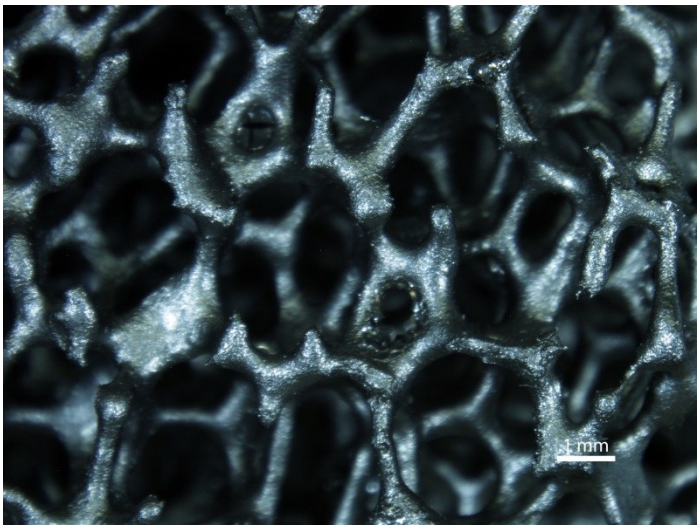

(a)

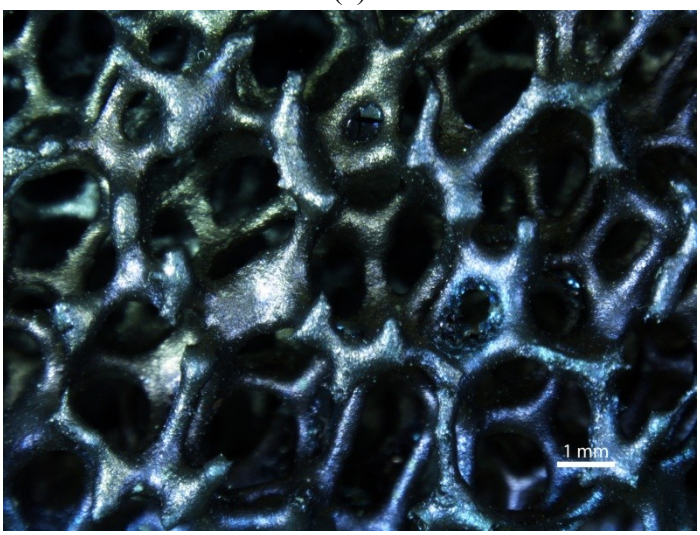

(b)

Figure 22 Stereomicroscope images of SiSiC (a) before and (b) after 200 thermal cycles at 1073 K (7.5x magnification)

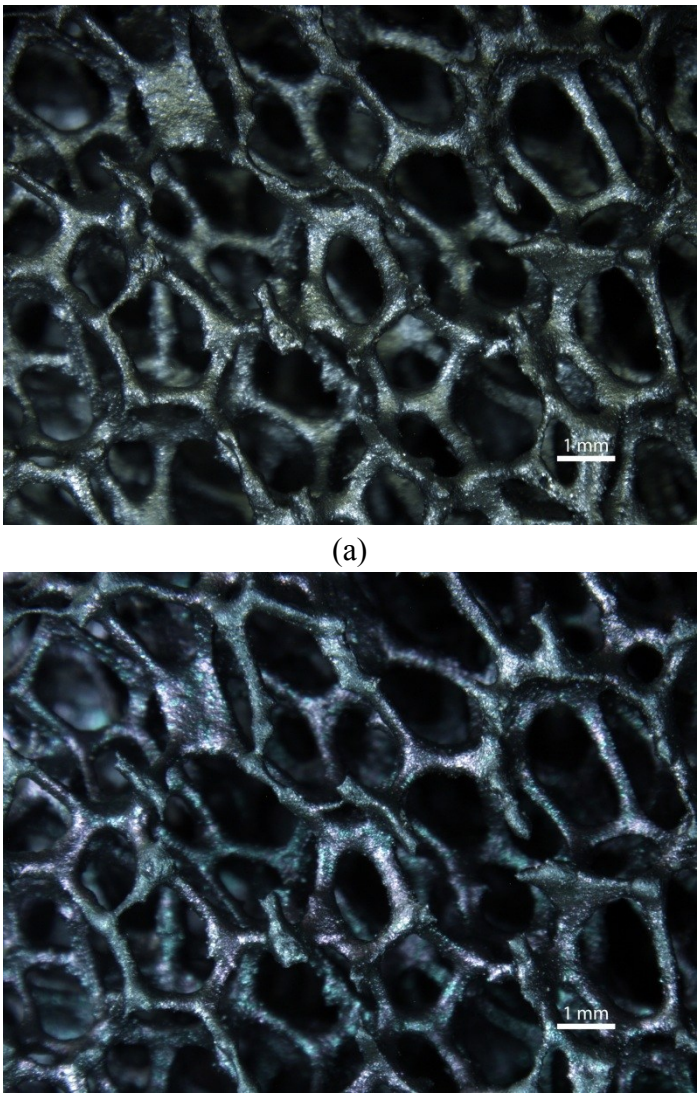

(a)

(b)

Figure 23 Stereomicroscope images of SiSiC (a) before and (b) after 200 thermal cycles at 1273 K (7.5x magnification)

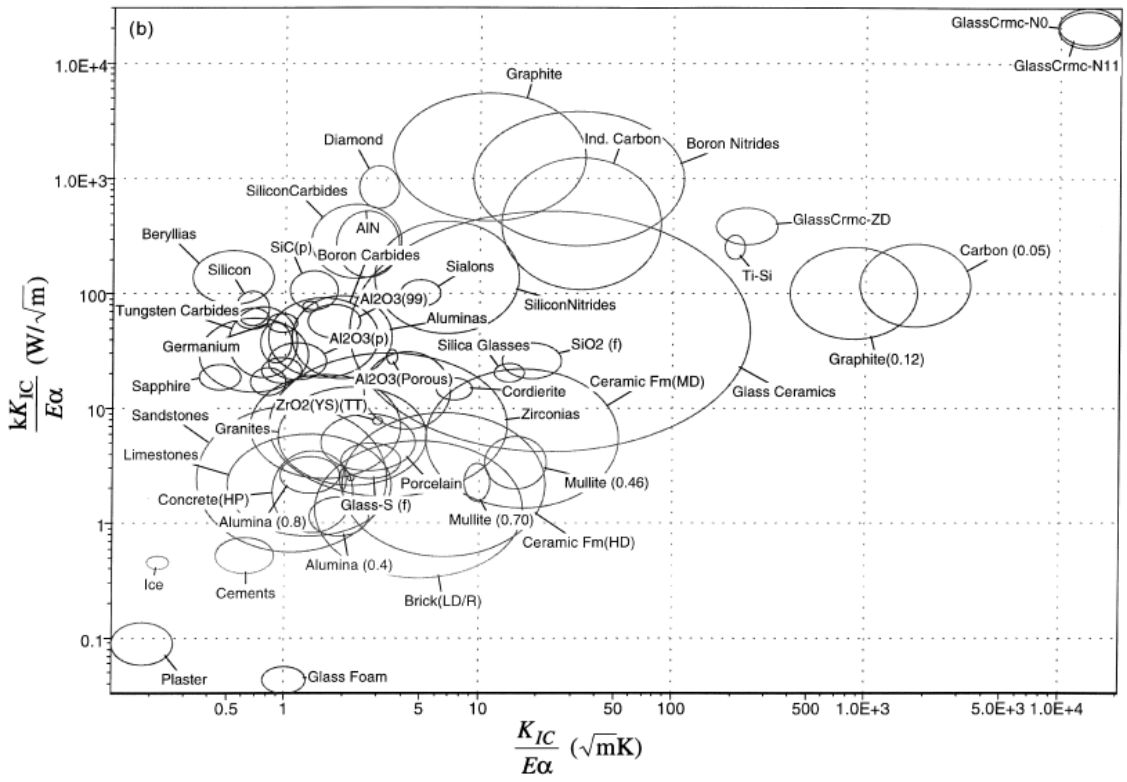

Figure 24 The merit indices for toughness-controlled failure $kK_{IC}/E\alpha$ vs $K_{IC}/E\alpha$, the top position lie for high resistance to thermal shock under poor heat transfer conditions while the right side lie for high thermal resistance to thermal shock under ideal heat transfer conditions.[27]

The Al_2O_3 sample after 200 cycles of thermal fatigue at 1073 K showed no macro-crack in the stereomicroscope observation (shown in Figure 25). However, Al_2O_3 sample after thermal fatigue at 1273 K develops three macro-cracks (two of them shown in Figure 26 and Figure 27). One of these cracks appeared after the first cycle. The number and length of the cracks increased as the number of cycles increased. During the thermal cycling, the material suffered thermal stress causing thermal strain in the strut. Increasing the number of cycles induced more strain in the strut. When the strain limit of material was reached, fracture occurred in the strut. The crack propagation stopped after 40 cycles when it reached the edge of the cuboid sample and connected to other cracks (Figure 28). For this

reason, we stopped the thermal fatigue experiment after 65 cycles. The low resistance of alumina foam to thermal fatigue was also reported by Venkata *et al.*[28] who found the strength reduction of the foam on the first cycle of thermal fatigue experiment at 1273 K. The strength reduction after the first cycle agrees with the crack development in our experiment. We conclude that Al_2O_3 foam develops macro-cracks on the first cycle of thermal fatigue at 1273 K.

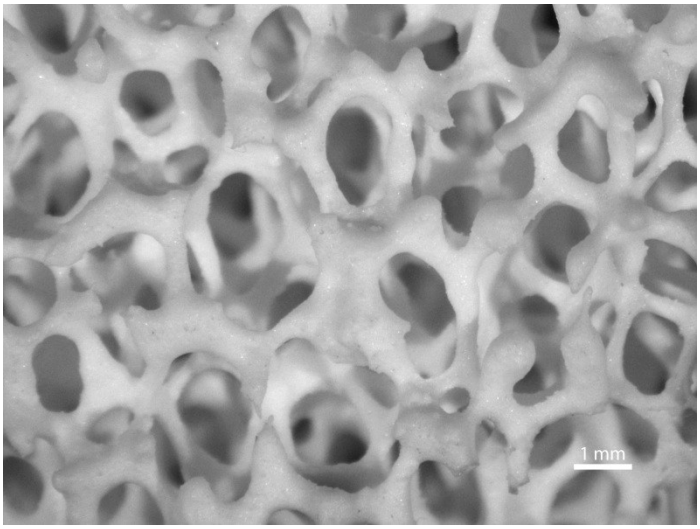

(a)

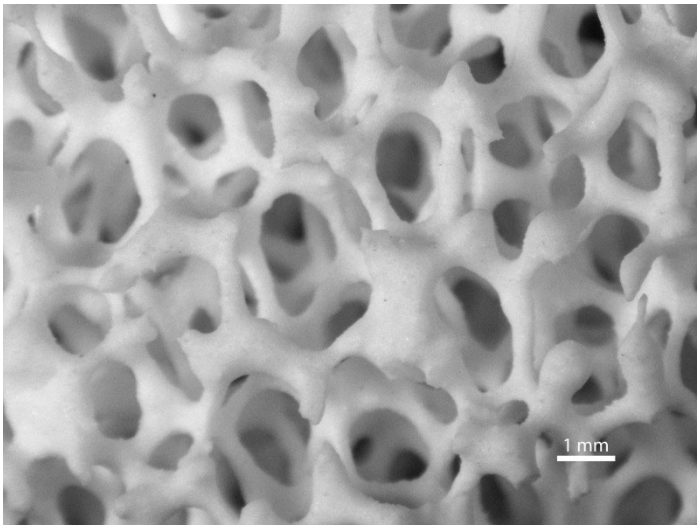

(b)

Figure 25 Stereomicroscope picture of Al_2O_3 (a) before and (b) after 200 thermal cycles at 1073 K (7.5x magnification)

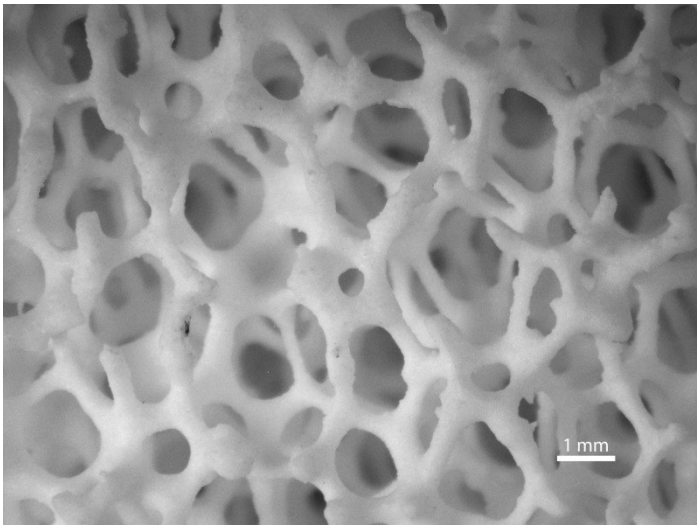

(a)

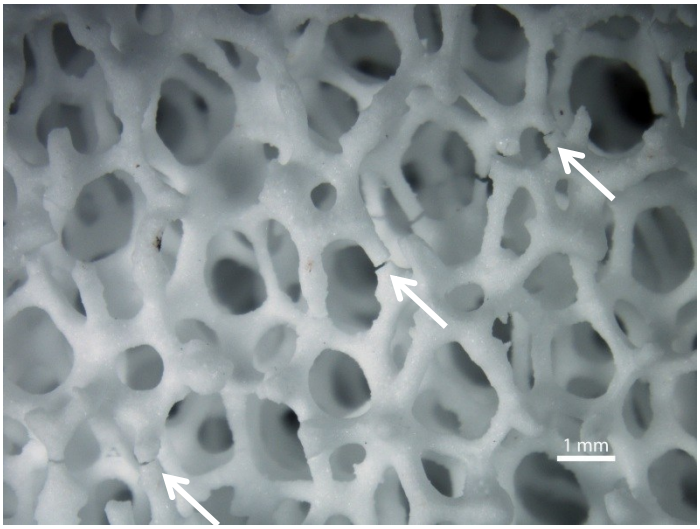

(b)

Figure 26 Stereomicroscope picture of Al_2O_3 on side 1 (a) before and (b) after 65 thermal cycles at 1273 K (7.5x magnification)

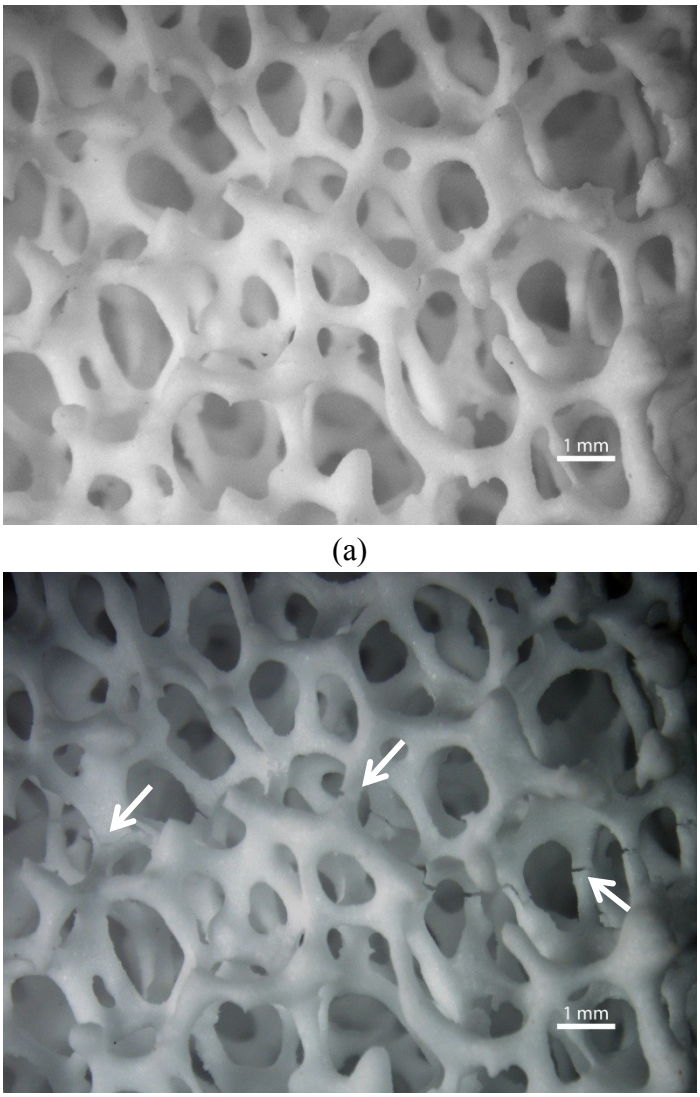

(a)

(b)

Figure 27 Stereomicroscope picture of Al_2O_3 on side 4 (a) before and (b) after 65 thermal cycles at 1273 K (7.5x magnification)

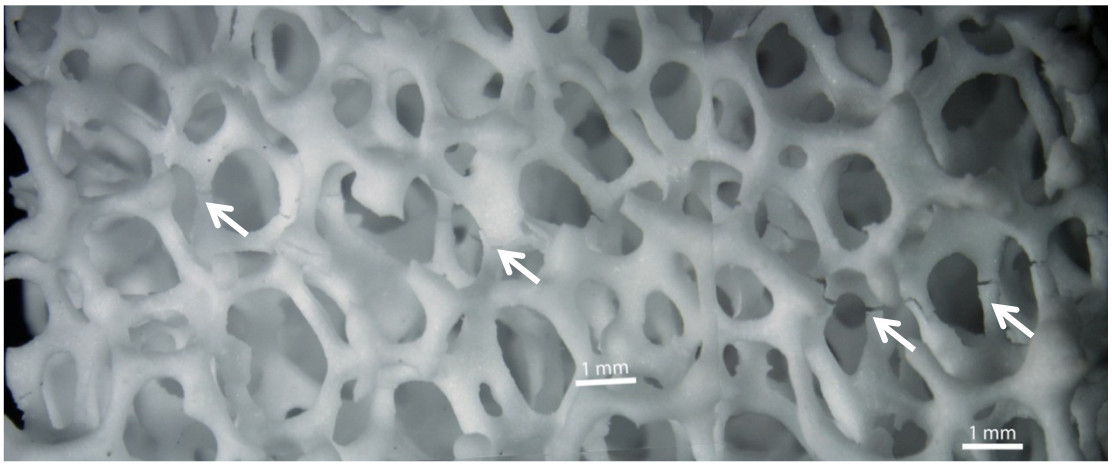

Figure 28 Stereomicroscope image of edge-to-edge crack in Al_2O_3 after 65 thermal cycles at 1273 K experiment on side 4

The length of three cracks of Al_2O_3 in each cycle were recorded and plotted as shown in Figure 29(a). Assuming the foam was isometric, the crack propagation followed order 3 of the following polynomial equation:

$$L = 6.98x10^{-5}N^3 - 0.0124N^2 + 0.754N + 0.624, \quad (14)$$

where L is the crack length and N is the number of cycles. Equation (14) calculates the crack length in the function of the number of cycles.

In Figure 29(b), we notice that the total crack surface area increases significantly up to 40 cycles before saturated. An increasing of cycles accumulates the thermal load, which causes cracks to propagate on the foam. Hence, it reduces surface area of the foam that sustains the thermal load normal to the crack orientation. After 40 cycles, the thermal stress presumably becomes lower than the stress required for crack propagation causing

no further damage in the sample. This saturation was also reported by Venkata *et al.* and M. C. Lu [28,29]. An equation is proposed to determine the specific surface area of the crack as a function of the number of cycles:

$$S = 0.00241 - 0.00237e^{-0.0547N}, \quad (15)$$

where the S is the crack surface area per volume of sample and N is the number of cycles. This equation (15) shows better relevance to the data plot than equation (14).

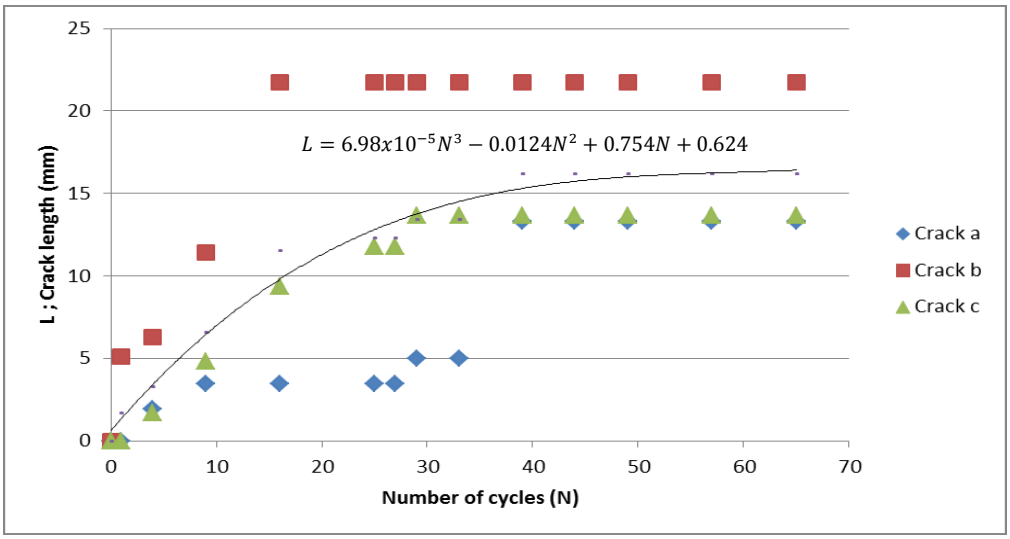

(a)

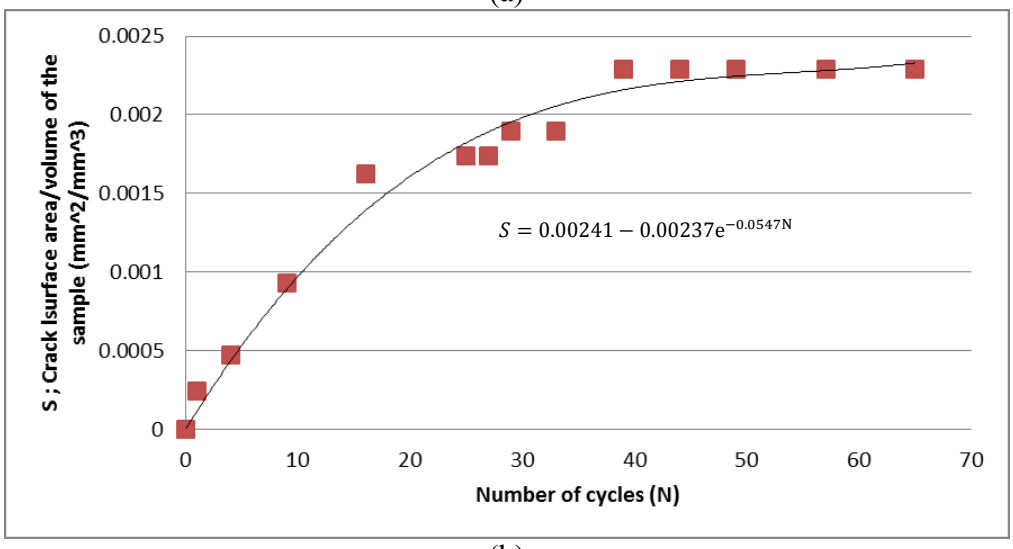

(b)

Figure 29 (a) crack length and (b) crack surface area per sample volume vs number of cycles for Al_2O_3 after thermal fatigue experiment at 1273 K.

4.4 Structural and Compositional Characterization

This section discusses about structural and phase composition analysis based on the X-Ray Diffraction results. The data were taken before and after the thermal fatigue experiment. The results of XRD on SiC sample (Figure 30) show that no significant difference in the peaks. Thus, there was no phase transformation during the experiment. The figure also shows that the SiC sample has a hexagonal crystal structure.

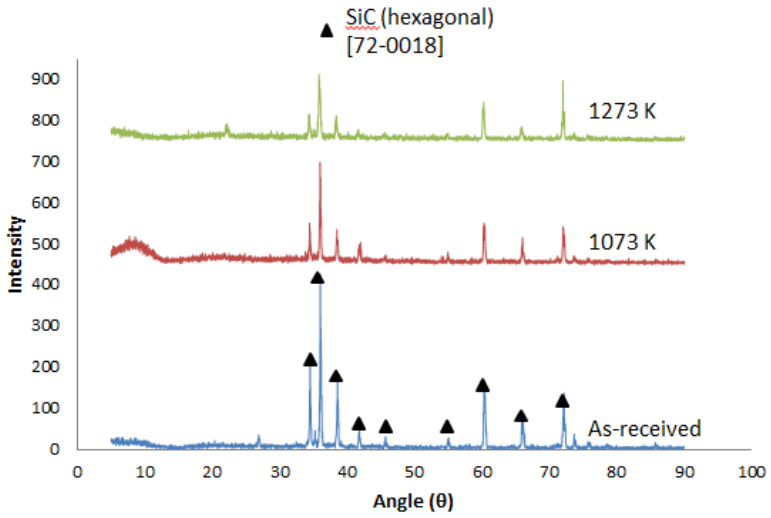

Figure 30 XRD patterns for as-received and after 200 thermal cycles performed at 1073 K and 1273 K for SiC

The XRD results in Figure 31 confirm that there are only two main materials in SiSiC sample, which are silicon metal and silicon carbide. This sample also did not have phase transformation during the experiment which explained by the same peak before and after the experiment. The silicon in the sample has a FCC crystal structure, while the SiC has a hexagonal structure.

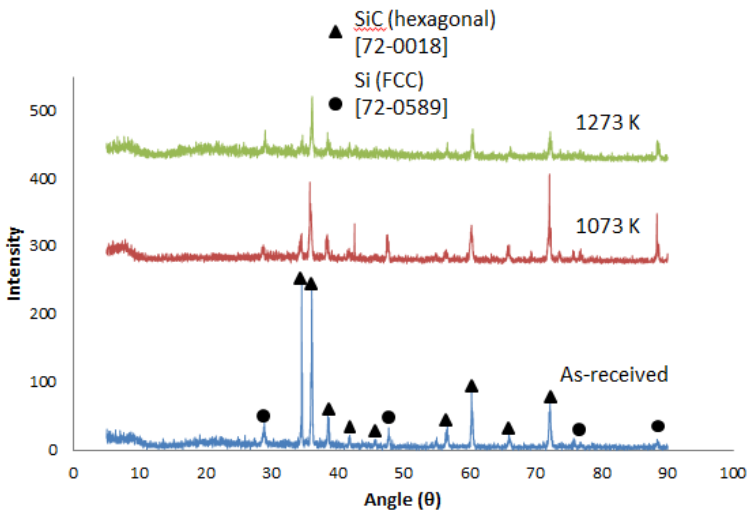

Figure 31 XRD patterns for as-received and after 200 thermal cycles performed at 1073 K and 1273 K for SiSiC

The XRD results for Al_2O_3 (Figure 32) also shows almost no phase transformation after the experiment. It can be seen that no additional element detected in the XRD pattern. The pattern also shows that Al_2O_3 sample had a rhombohedral crystal structure, which confirms the presence of alpha-alumina (α-Al_2O_3) phase.

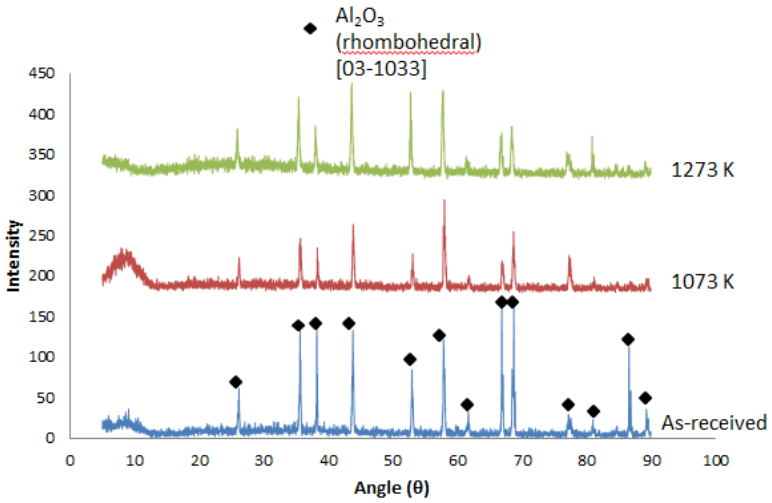

Figure 32 XRD patterns for as-received and after thermal cycle experiments performed at 1073 K and 1273 K for Al_2O_3

4.5 Morphological and Compositional Characterization

4.5.1 Foam Morphological Images

The morphological of foam were evaluated using SEM imaging with low magnification (25-27x), to capture the strut and the cell morphology. The images of SiC and Al_2O_3 in Figure 33 show that their struts have big pores/holes inside it. These pores certainly have effect to the strength of the strut and the effective thermal conductivity within the strut. The pore in Al_2O_3 might contribute to the reasons why it easily cracks at 1273 K compare to SiC and SiSiC sample. The only sample that does not have pores inside the strut is SiSiC (as seen in Figure 33), because the pores were filled with silicon metal during its manufacturing method.[30] As for SiSiC, the free silicon metal and the solid structure inside the strut are additional factors that increase thermal fatigue resistance of this foam.

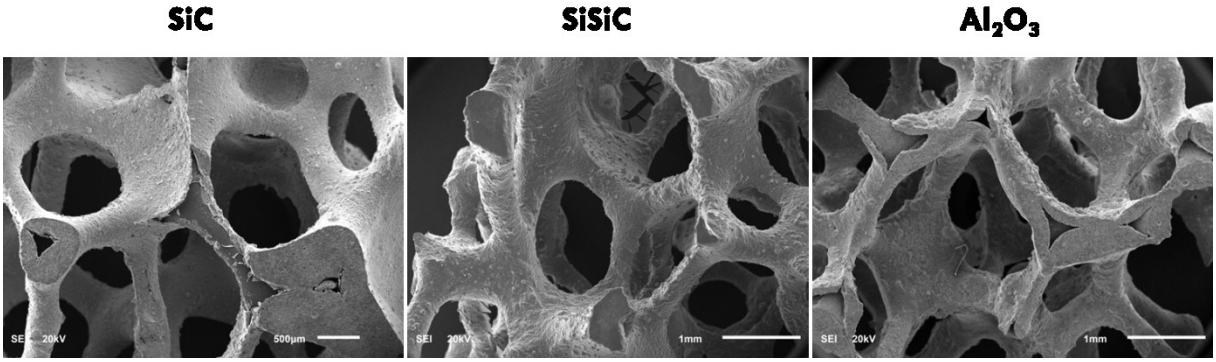

Figure 33 SEM images of the foam at SiC, SiSiC and Al_2O_3 (left to right).

4.5.2 Strut Surface Morphology and Elemental Analysis

We observed the surface morphology of all samples using SEM imaging with 1000x magnification. In this magnification, we could see the surface and grain morphology of the material. In Figure 34-36, it is clear that no morphological change detected after thermal fatigue experiment for all samples at both 1073 K and 1273 K.

As we know, the Al_2O_3 at 1073 K does not show any macro-cracks after thermal cycle up to 200 cycles. However, Figure 37 shows there is a micro-crack that propagated through thickness of a strut in the sample. This crack might be an initial crack which not developed further in the specimen. It shows that the crack did not fully separate the strut. This is an indication that Al_2O_3 sample developed micro-crack at 1073 K. The temperature difference and 200 cycles were not enough to force propagation of the crack through other strut. Therefore, the crack was not seen in the stereomicroscope. Considering the macro-cracks occurred at 1273 K, we might expect the development of micro-crack to macro-crack takes place between temperatures 1073 K to 1273 K.

The EDS were used to confirm the element of the material before and after the experiment. The EDS results of SiC and SiSiC samples (Figure 38 and Figure 39) show that there is another element detected in the sample, which is oxygen. The oxygen detection comes from silicon oxide (SiO_2) compound, which is already there before the treatment as explained by the supplier. The reason it was not appear in the XRD because it has amorphous structure. Since SiO_2 was there even in the as-received sample, we could confirm that both of the materials did not have phase transformation during the thermal fatigue experiment.

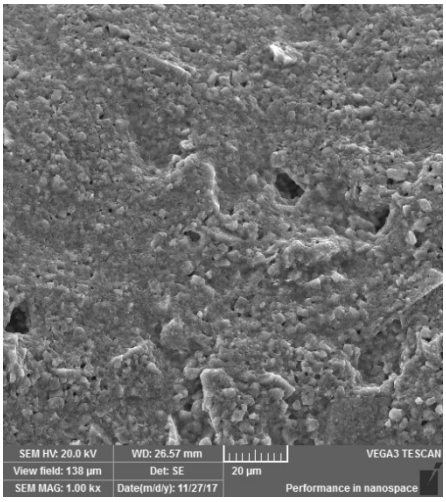

(a)

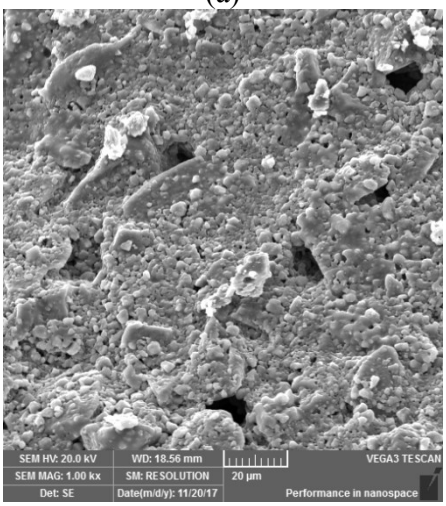

(b)

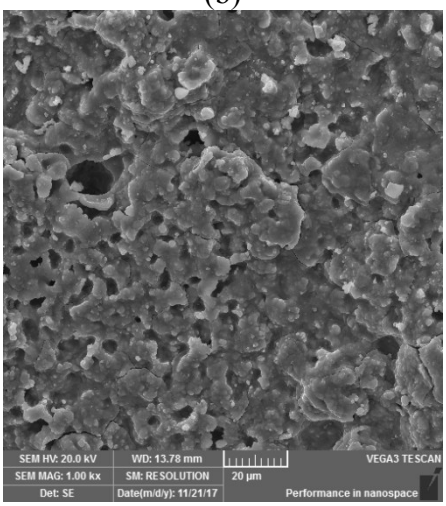

(c)

Figure 34 SEM of SiC sample at 1000x magnification, (a) as received (b) 1073 K (c) 1273 K.

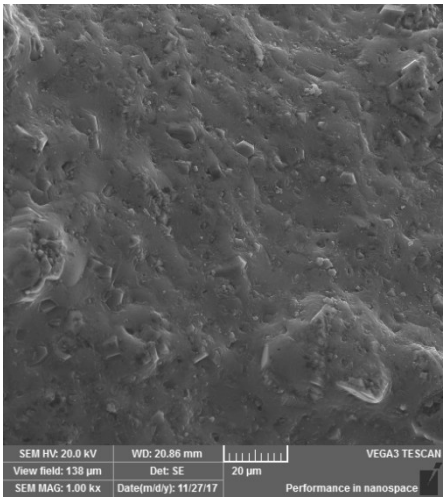

(a)

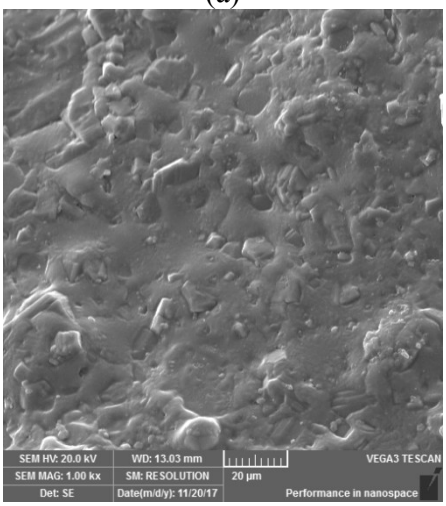

(b)

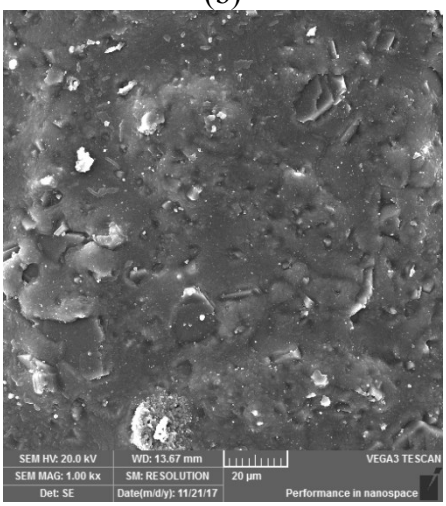

(c)

Figure 35 SEM of SiSiC sample at 1000x magnification, (a) as received (b) 1073 K (c) 1273 K

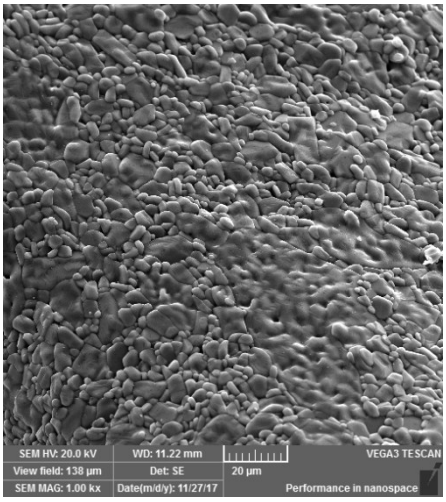

(a)

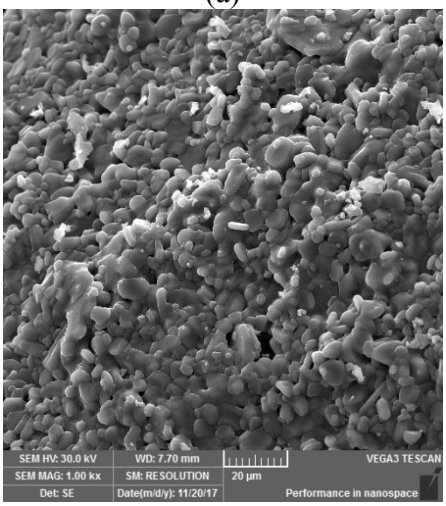

(b)

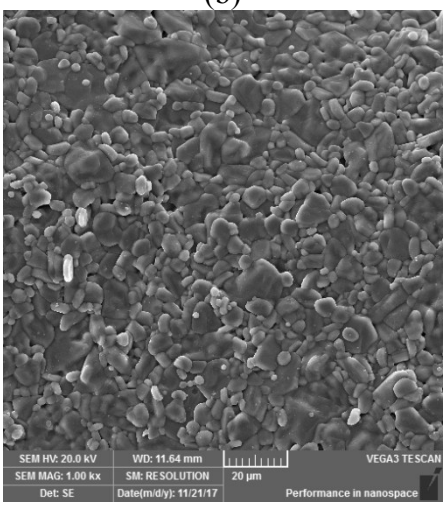

(c)

Figure 36 SEM of Al_2O_3 sample at 1000x magnification, (a) as received (b) 1073 K (c) 1273 K

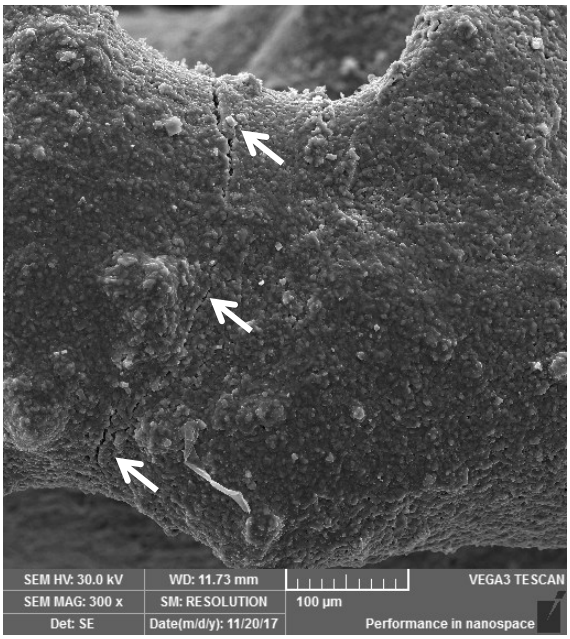

Figure 37 A through strut thickness micro-crack found on the Al_2O_3 sample after 200 thermal cycles at 1073 K.

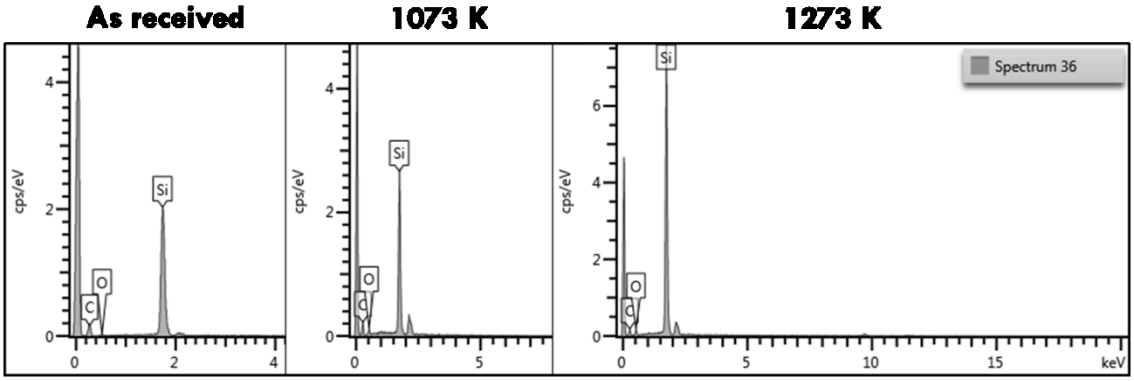

Figure 38 EDS analysis for as received and after thermal cycle experiments performed at 1073 K and 1273 K for SiC sample

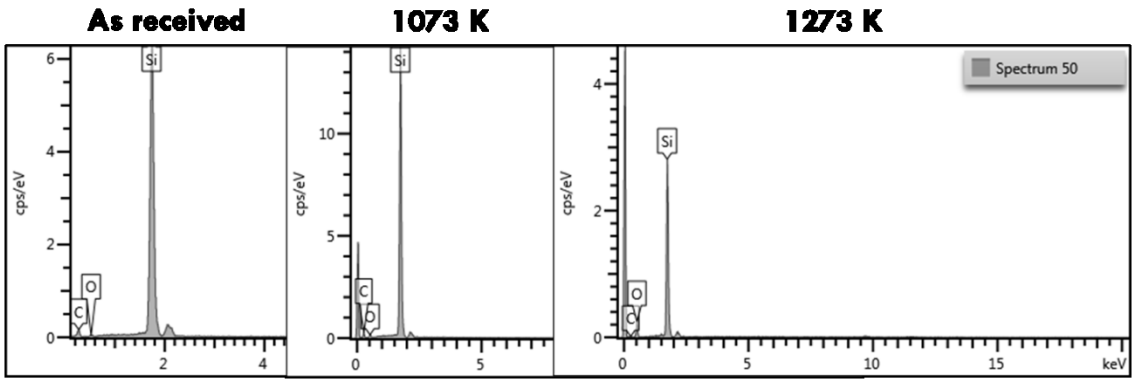

Figure 39 EDS analysis for as received and after thermal cycle experiments performed at 1073 K and 1273 K for SiSiC sample

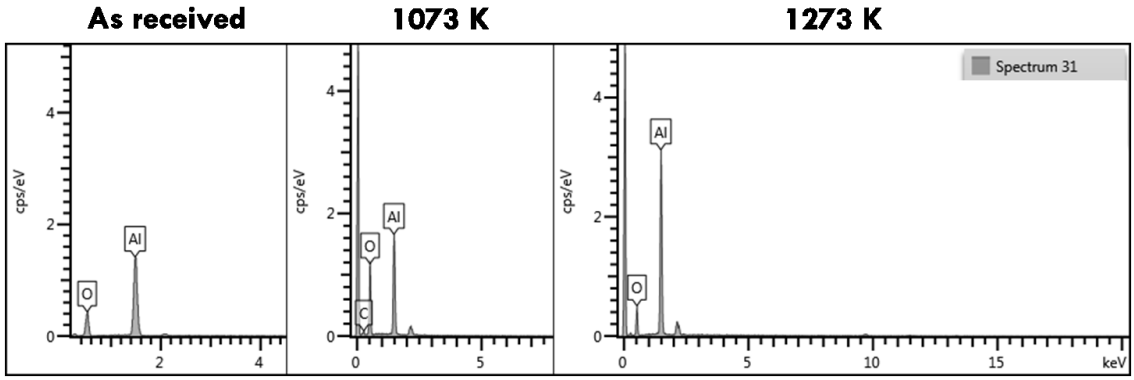

Figure 40 EDS analysis for as received and after thermal cycle experiments performed at 1073 K and 1273 K for Al_2O_3 sample

As for Al_2O_3, it is clear that the sample has aluminum and oxygen. The quantitative result from EDS analysis were shown in Table 7. It was confirmed that the alumina sample has right empirical formula Al_2O_3.

Table 7 Quantitative analysis of Al_2O_3 sample

Sample	Element	Atomic weight	Weight (%)	Smallest ratio	Empirical formula
As-received	O	16.00	46.41	1.46	3
	Al	26.98	53.59	1.00	2
1073 K	O	16.00	42.77	1.26	3
	Al	26.98	57.23	1.00	2
1273 K	O	16.00	46.95	1.49	3
	Al	26.98	53.05	1.00	2

These EDS and SEM images confirmed the XRD results that show no phase transformation detected in all sample compositions. Thus, all of samples were chemically stable after 200 cycles of thermal fatigue at 1073 K and 1273 K.

CHAPTER 5

CONCLUSION AND RECOMMENDATION

5.1 Conclusion

The conclusions of the thesis are summarized in the following sentences;

a. Maximum and minimum flow-rate estimated were 14 L/s and 33 L/s respectively for 20 kW receiver.
b. An experimental design was established, a receiver was manufactured, and three materials were selected for the real condition experiment.
c. A thermal fatigue experiment was conducted to Al_2O_3, SiC, and SiSiC foams at temperatures 1073 K and 1273 K up to 200 cycles.
d. A micro-crack was observed by SEM on the Al_2O_3 after 200 thermal cycles at 1073 K. Three macro-cracks were observed in the Al_2O_3 after thermal cycles at 1273 K. The macro-crack appeared at first cycle and propagated to the other edge of the sample at 25th cycle.
e. No crack was observed in the SiC and SiSiC after 200 thermal cycles at 1073 K and 1273 K.
f. The effective thermal conductivity results of all materials showed no significant changes after the thermal fatigue experiment.

g. The XRD, SEM, and EDS results showed no changes in the phase composition and morphology of all materials; Al_2O_3, SiC, and SiSiC.
h. The SiC and SiSiC foams are the best candidates for the application due to high resistance to crack during thermal fatigue experiment.

5.2 Recommendation

Further researches are needed to understand how the material properties affect the performance of solar absorber. Therefore, the following recommendations were proposed;

a. Several new material candidates for the absorber application have better performance than SiC and SiSiC.
b. The possibility to use another type of absorber structure is possible.
c. Higher temperature and number of cycles for thermal fatigue experiment are needed to evaluate the maximum operating temperature and maximum fatigue life of the absorber.
d. Acoustics Emission method to measure the mechanical properties of sample is needed to support quantitatively degradation of the material due to thermal fatigue.
e. Running the experiment in the real condition will produce real-time and reliable data hence could provide better understanding of the phenomenon inside the absorber.

APPENDICES

A. Thermal conductivity of Al_2O_3 at different temperature

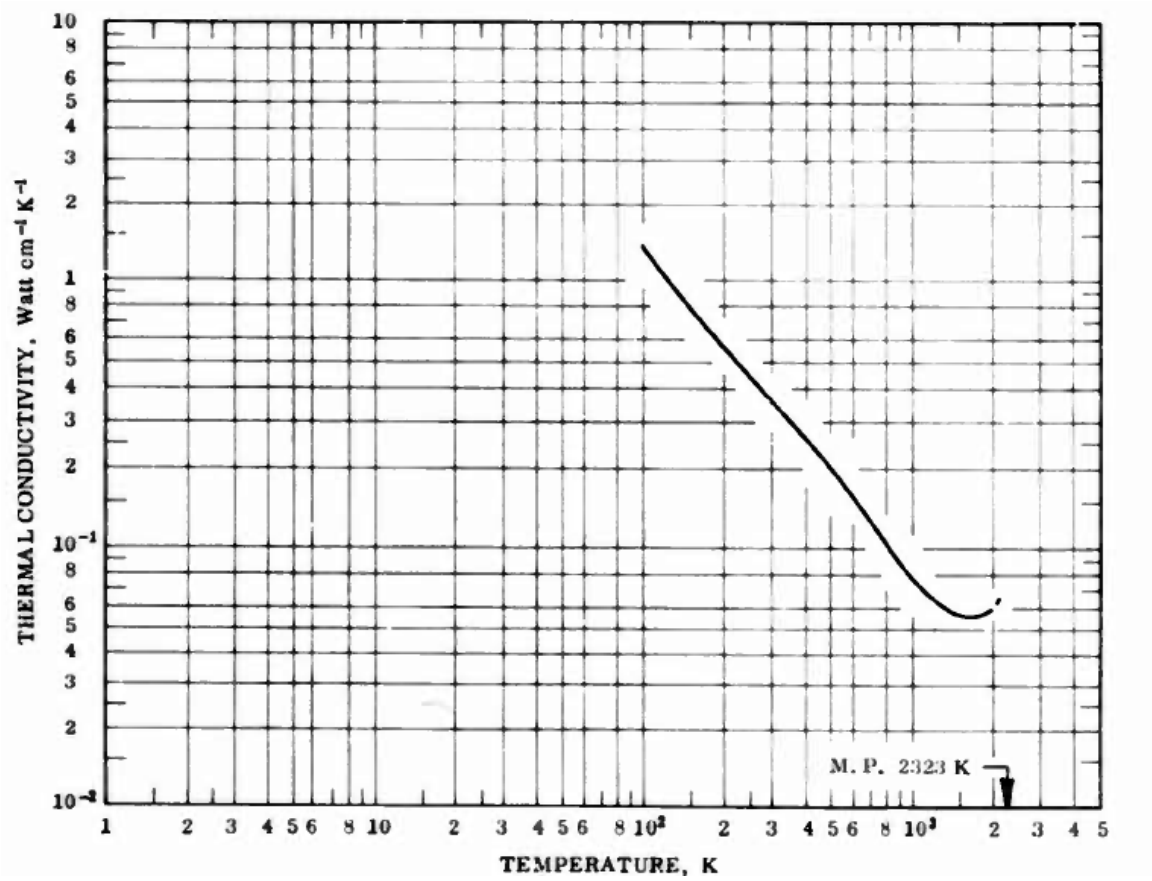

REMARKS

The recommended values are for 99.5% pure, 98% dense, polycrystalline Al_2O_3. The recommended values are thought to be accurate to within 6% of the true values at temperatures from 500 to 1000 K and 6 to 10% at other temperatures.

RECOMMENDED VALUES*

(For 99.5% pure, 98% dense, polycrystalline Al_2O_3)

T_1	k_1	k_2	T_2
0	0	0	-459.7
100	1.33	76.9	-279.7
150	0.77	44.5	-189.7
200	0.55	31.8	- 99.7
250	0.434	25.1	- 9.7
273.2	0.397	22.9	32.0
300	0.360	20.8	80.3
350	0.307	17.7	170.3
400	0.264	15.3	260.3
500	0.202	11.7	440.3
600	0.158	9.13	620.3
700	0.126	7.28	800.3
800	0.104	6.01	980.3
900	0.089	5.14	1160
1000	0.0785	4.54	1340
1100	0.0710	4.10	1520
1200	0.0655	3.79	1700
1300	0.0613	3.54	1880
1400	0.0583	3.37	2060
1500	0.0566	3.27	2240
1600	0.0556	3.21	2420
1700	0.0554	3.20	2600
1800	0.0559	3.23	2780
1900	0.0574	3.32	2960
2000	0.0600	3.47	3140
2100	(0.0644) ‡	(3.72)	3320

Data taken from Y. S. Touloukian, R. W. Powell, C. Y. Ho, and P. G. Klemens, *Thermophysical Properties of Matter -The TPRC Data Series- Vol. 2. Thermal Conductivity - Nonmetallic Solids*.

B. Thermal expansion of Al_2O_3 at different temperature

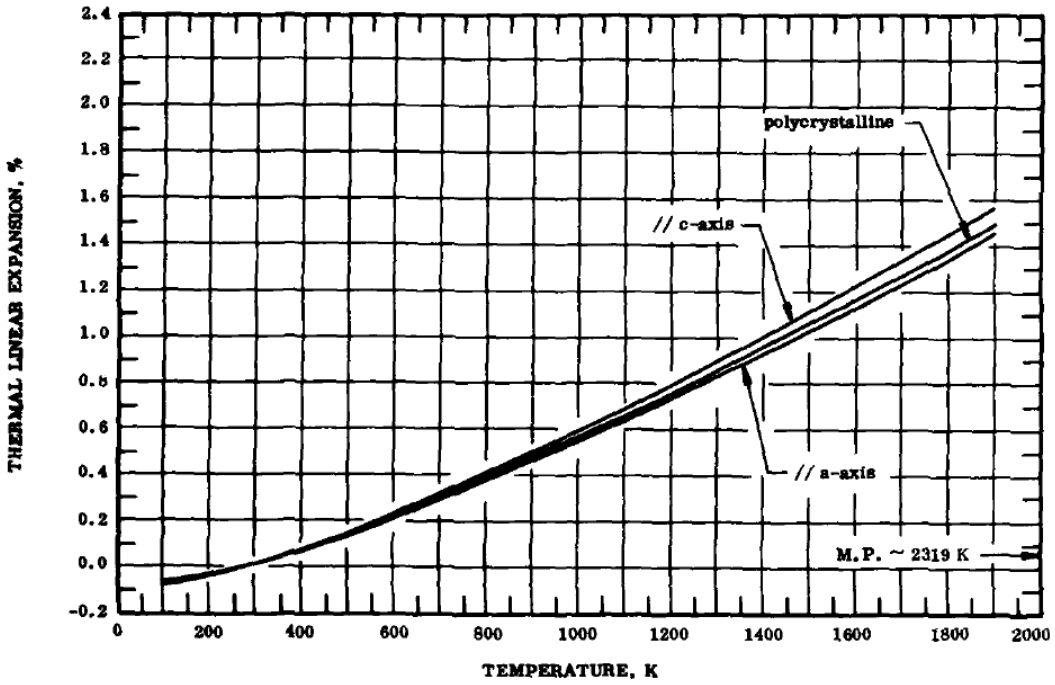

REMARKS

The recommended values for the axial thermal expansion are based on the data for pure samples. The values for the polycrystalline sample are calculated from the axial values. These values are considered accurate to within ±3% and are represented approximately by the following equation:

// c-axis:	$\Delta L/L_0 = -0.115 + 3.772 \times 10^{-4} T - 1.999 \times 10^{-7} T^2 + 8.416 \times 10^{-10} T^3$	(100-293 K)
	$\Delta L/L_0 = -0.192 + 5.927 \times 10^{-4} T + 2.142 \times 10^{-7} T^2 - 2.207 \times 10^{-11} T^3$	(293-1900 K)
// a-axis:	$\Delta L/L_0 = -0.124 + 1.056 \times 10^{-3} T - 5.175 \times 10^{-6} T^2 + 1.030 \times 10^{-8} T^3$	(100-293 K)
	$\Delta L/L_0 = -0.176 + 5.431 \times 10^{-4} T + 2.150 \times 10^{-7} T^2 - 2.810 \times 10^{-11} T^3$	(293-1900 K)
polycrystalline:	$\Delta L/L_0 = -0.121 + 8.303 \times 10^{-4} T - 3.519 \times 10^{-6} T^2 + 7.152 \times 10^{-9} T^3$	(100-293 K)
	$\Delta L/L_0 = -0.180 + 5.494 \times 10^{-4} T + 2.252 \times 10^{-7} T^2 - 2.894 \times 10^{-11} T^3$	(293-1900 K)

The tabulated values for the coefficient of thermal expansion are derived from the experimental data and are considered accurate to about ±.%.

RECOMMENDED VALUES

[Temperature, T, K; Linear Expansion, $\Delta L/L_0$, %; α, 10^{-6} K^{-1}]

	// c-axis	// a-axis	polycrystalline	
T	$\Delta L/L_0$	$\Delta L/L_0$	$\Delta L/L_0$	α
100	-0.078	-0.060	-0.066	0.6
150	-0.060	-0.047	-0.051	1.9
200	-0.040	-0.037	-0.038	3.3
250	-0.020	-0.022	-0.021	4.5
293	0.000	0.000	0.000	5.4
400	0.078	0.073	0.075	7.1
500	0.155	0.145	0.148	7.5
600	0.236	0.220	0.225	7.9
700	0.320	0.300	0.305	8.2
800	0.408	0.380	0.388	8.5
900	0.500	0.465	0.476	8.8
1000	0.593	0.552	0.565	9.1
1100	0.690	0.644	0.658	9.4
1200	0.790	0.736	0.754	9.6
1300	0.892	0.830	0.852	9.9
1400	0.998	0.928	0.952	10.1
1500	1.105	1.027	1.054	10.3
1600	1.215	1.128	1.158	10.5
1700	1.325	1.230	1.263	10.6
1800	1.440	1.333	1.370	10.9
1900	1.555	1.440	1.480	11.0

Data taken from Y. S. Touloukian, R. K. Kirby, R. E. Taylor, and T. Y. Lee, *Thermophysical Properties of Matter -The TPRC Data Series- Vol. 13. Thermal Epansion - Nonmetallic Solids*.

C. The drawing of receiver parts

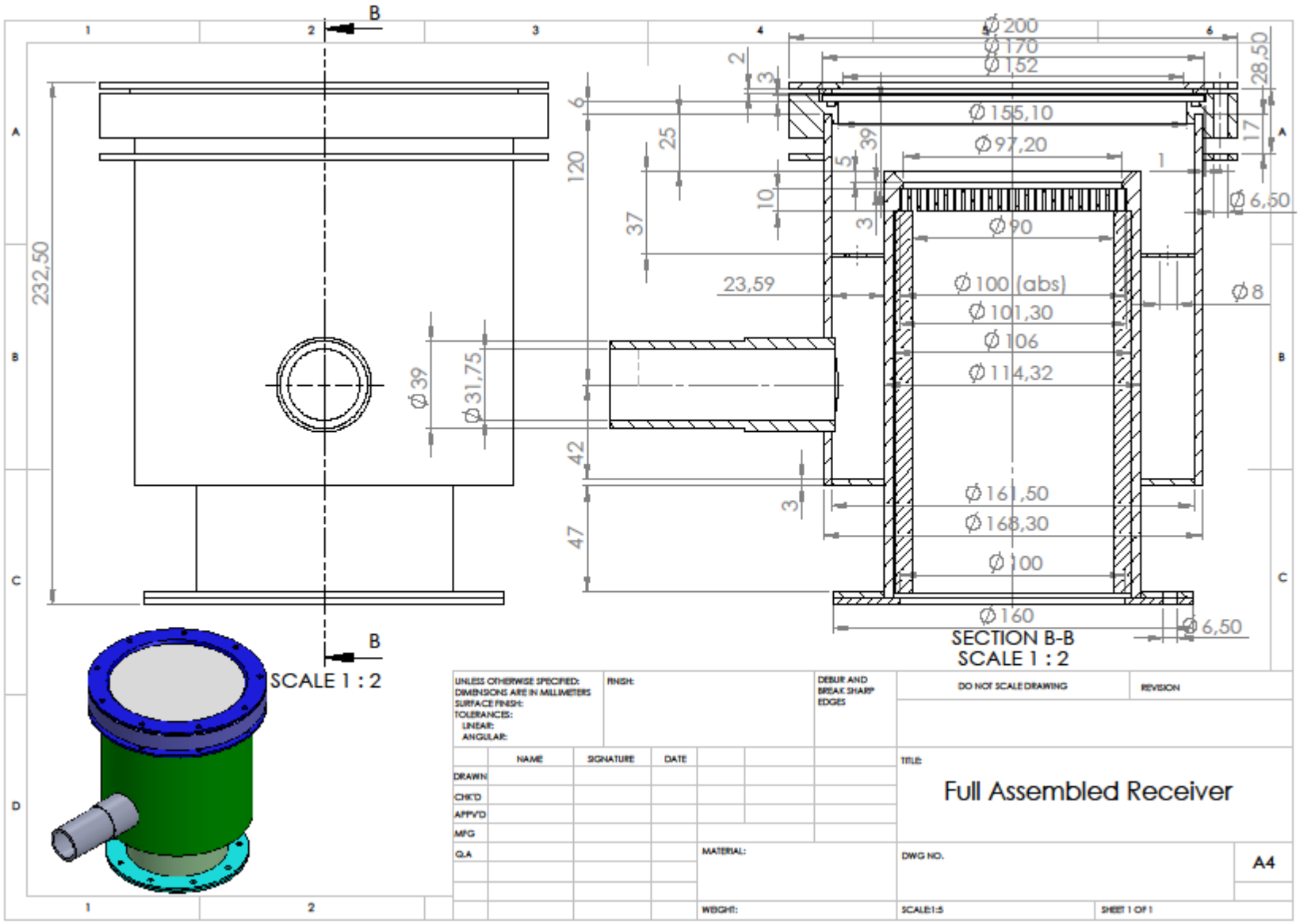
B
B
232,50
Ø 39
Ø 31,75
SCALE 1 : 2
Ø 200
Ø 170
Ø 152
Ø 155,10
Ø 97,20
Ø 90
Ø 100 (abs)
Ø 101,30
Ø 106
Ø 114,32
Ø 161,50
Ø 168,30
Ø 100
Ø 160
Ø 6,50
Ø 8
2
3
6
120
25
37
10
5
39
3
23,59
42
3
47
28,50
17
1
SECTION B-B
SCALE 1 : 2
UNLESS OTHERWISE SPECIFIED:
DIMENSIONS ARE IN MILLIMETERS
SURFACE FINISH:
TOLERANCES:
LINEAR:
ANGULAR:
FINISH:
DEBUR AND BREAK SHARP EDGES
DO NOT SCALE DRAWING
REVISION
NAME
SIGNATURE
DATE
DRAWN
CHK'D
APPV'D
MFG
QA
MATERIAL:
WEIGHT:
TITLE:
Full Assembled Receiver
DWG NO.
A4
SCALE:1:5
SHEET 1 OF 1

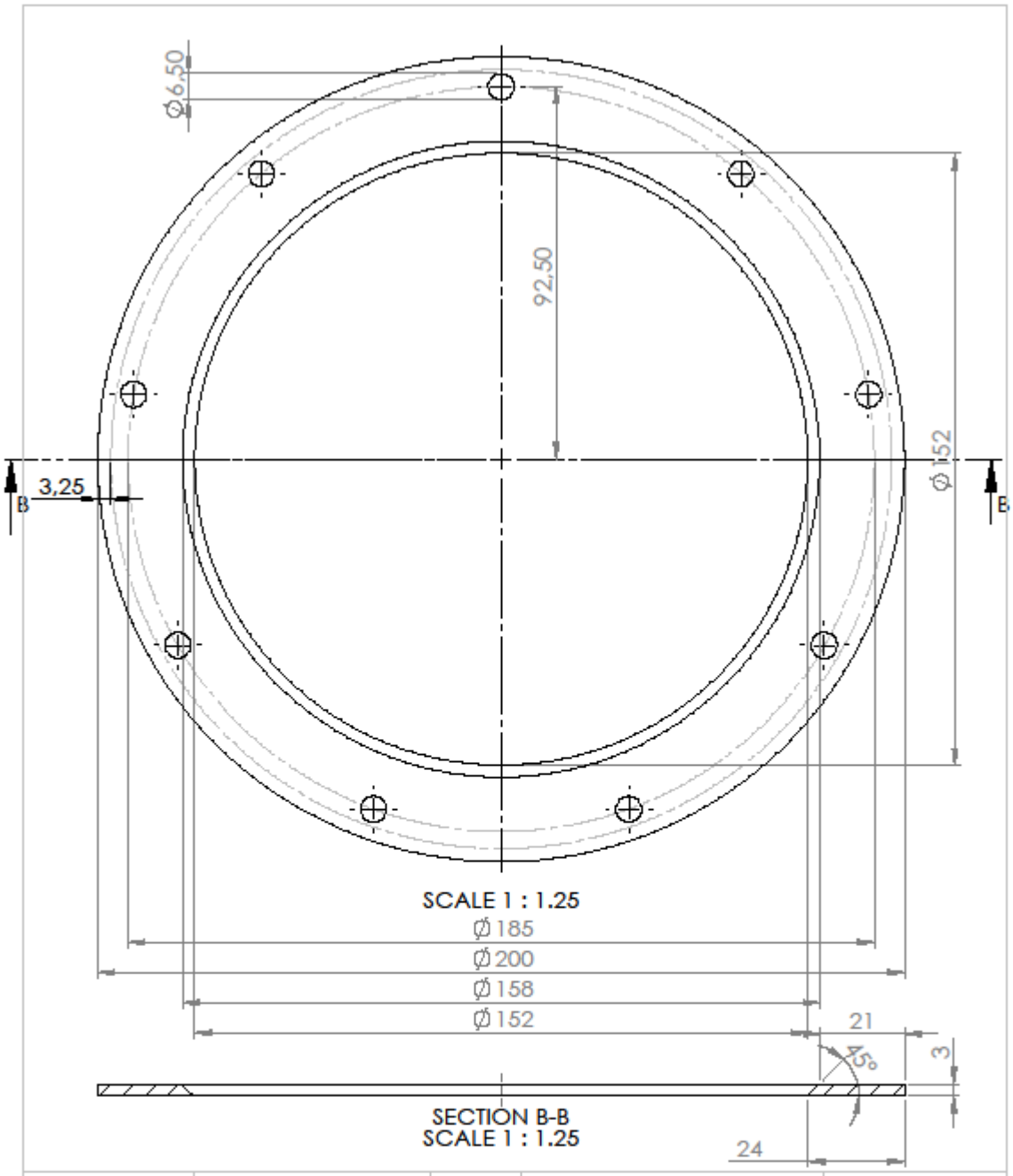

UNLESS OTHERWISE SPECIFIED: DIMENSIONS ARE IN MILLIMETERS SURFACE FINISH: TOLERANCES: LINEAR: ANGULAR:	FINISH:		DEBUR AND BREAK SHARP EDGES	DO NOT SCALE DRAWING	REVISION
	NAME	SIGNATURE	DATE	TITLE:	
DRAWN				Part 1-Glass Cover upper part	
CHK'D					
APPV'D					
MFG					
Q.A			MATERIAL:	DWG NO.	A4
			WEIGHT:	SCALE:1:5	SHEET 1 OF 1

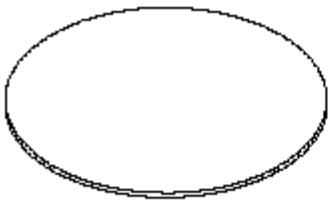

SCALE 1 : 3

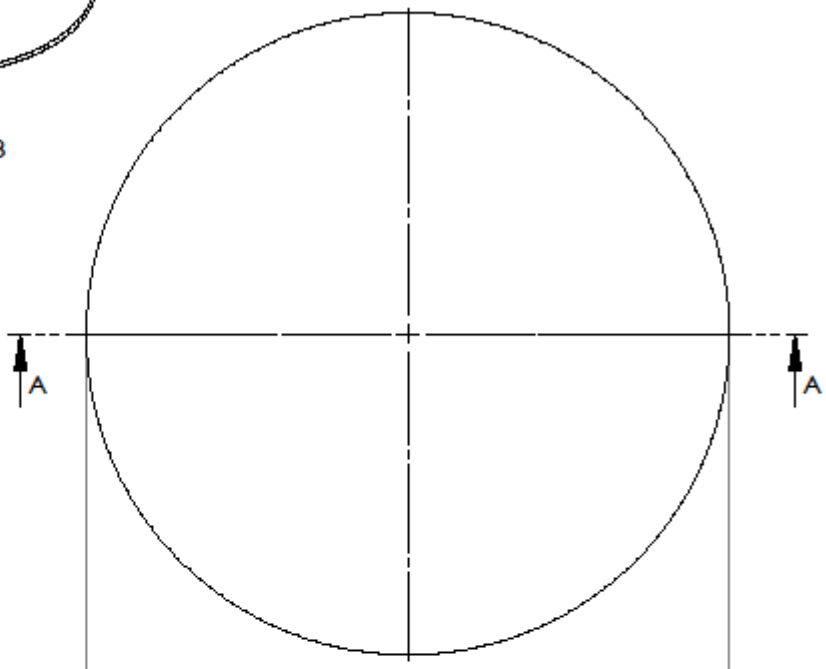

SCALE 1 : 1.5

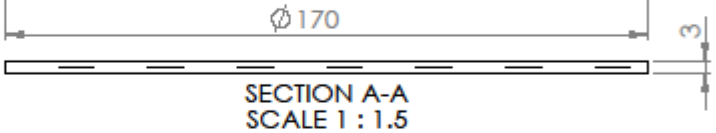

SECTION A-A
SCALE 1 : 1.5

UNLESS OTHERWISE SPECIFIED: DIMENSIONS ARE IN MILLIMETERS SURFACE FINISH: TOLERANCES: LINEAR: ANGULAR:		FINISH:				DEBUR AND BREAK SHARP EDGES	DO NOT SCALE DRAWING	REVISION
	NAME	SIGNATURE	DATE				TITLE: Part 2 - Flat Glass	
DRAWN								
CHK'D								
APPV'D								
MFG								
Q.A				MATERIAL:			DWG NO.	A4
				WEIGHT:			SCALE:1:5	SHEET 1 OF 1

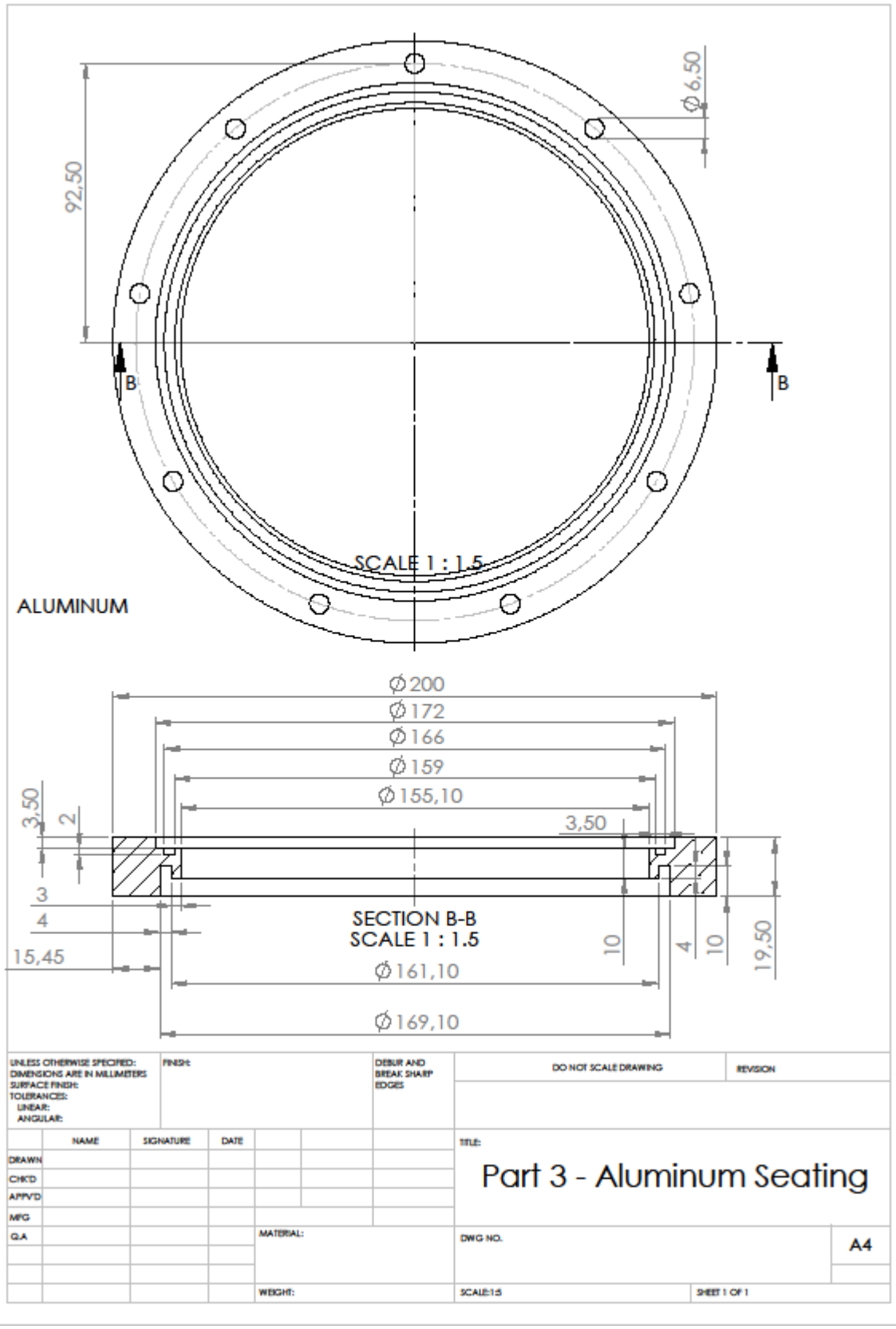
92,50
Ø6,50
B
B
SCALE 1 : 1.5
ALUMINUM
Ø200
Ø172
Ø166
Ø159
Ø155,10
3,50
2
3,50
3
4
15,45
SECTION B-B
SCALE 1 : 1.5
10
4
10
19,50
Ø161,10
Ø169,10
UNLESS OTHERWISE SPECIFIED:
DIMENSIONS ARE IN MILLIMETERS
SURFACE FINISH:
TOLERANCES:
LINEAR:
ANGULAR:
FINISH:
DEBUR AND BREAK SHARP EDGES
DO NOT SCALE DRAWING
REVISION
NAME
SIGNATURE
DATE
DRAWN
CHK'D
APPV'D
MFG
Q.A
MATERIAL:
WEIGHT:
TITLE:
Part 3 - Aluminum Seating
DWG NO.
A4
SCALE:1:5
SHEET 1 OF 1

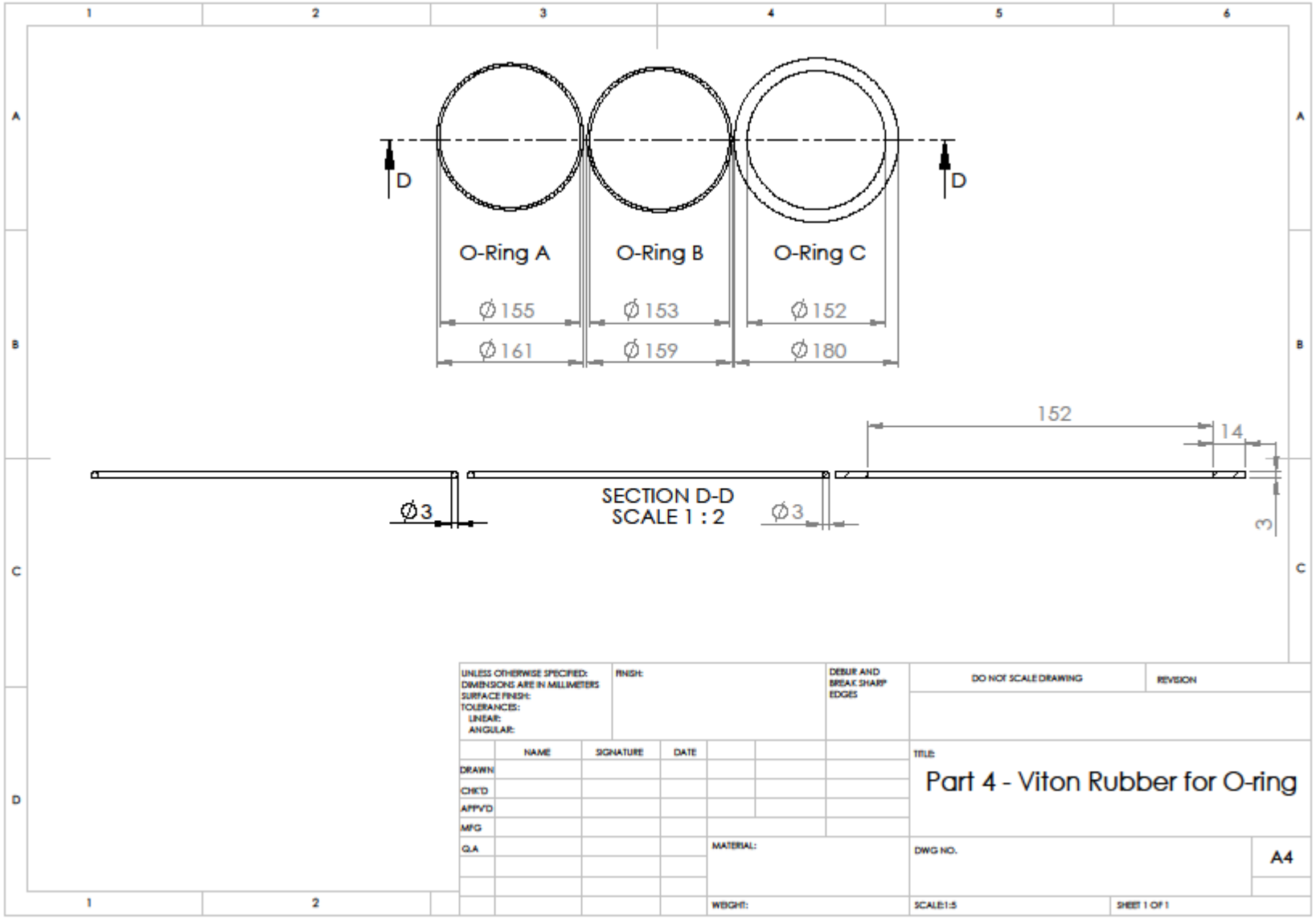
D
D
O-Ring A
O-Ring B
O-Ring C
Ø155
Ø153
Ø152
Ø161
Ø159
Ø180
152
14
3
Ø3
SECTION D-D
SCALE 1 : 2
Ø3
UNLESS OTHERWISE SPECIFIED:
DIMENSIONS ARE IN MILLIMETERS
SURFACE FINISH:
TOLERANCES:
LINEAR:
ANGULAR:
FINISH:
DEBUR AND BREAK SHARP EDGES
DO NOT SCALE DRAWING
REVISION
NAME
SIGNATURE
DATE
DRAWN
CHK'D
APPV'D
MFG
QA
MATERIAL:
WEIGHT:
TITLE:
Part 4 - Viton Rubber for O-ring
DWG NO.
A4
SCALE:1:5
SHEET 1 OF 1

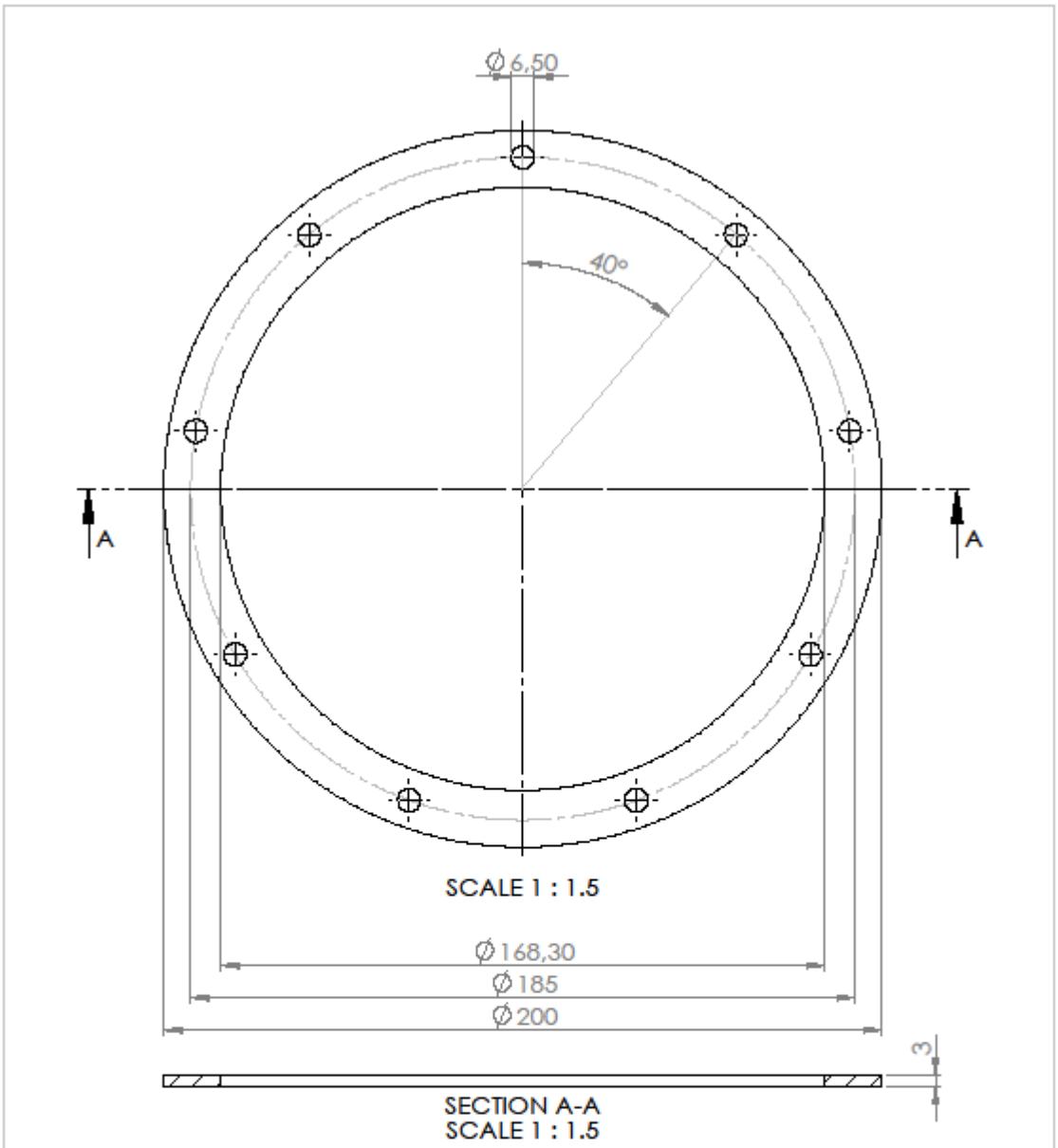

UNLESS OTHERWISE SPECIFIED: DIMENSIONS ARE IN MILLIMETERS SURFACE FINISH: TOLERANCES: LINEAR: ANGULAR:		FINISH:		DEBUR AND BREAK SHARP EDGES		DO NOT SCALE DRAWING	REVISION
	NAME	SIGNATURE	DATE			TITLE:	
DRAWN						Part 5 - Glass Cover Lower Part	
CHK'D							
APPV'D							
MFG							
Q.A				MATERIAL:		DWG NO.	A4
				WEIGHT:		SCALE:1:5	SHEET 1 OF 1

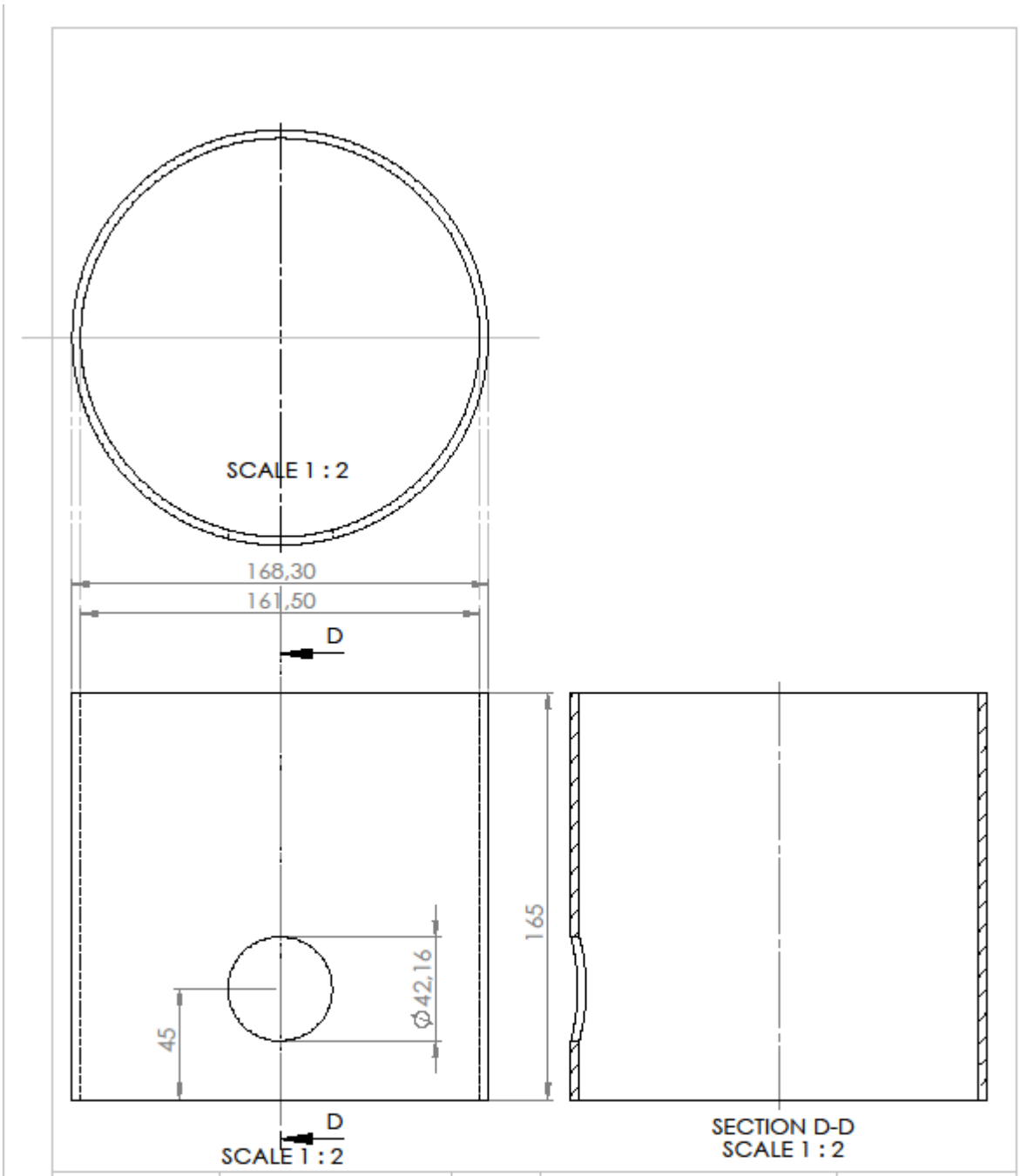
SCALE 1 : 2
168,30
161,50
D
165
Ø42,16
45
D
SCALE 1 : 2
SECTION D-D
SCALE 1 : 2
UNLESS OTHERWISE SPECIFIED:
DIMENSIONS ARE IN MILLIMETERS
SURFACE FINISH:
TOLERANCES:
LINEAR:
ANGULAR:
FINISH:
DEBUR AND BREAK SHARP EDGES
DO NOT SCALE DRAWING
REVISION
NAME
SIGNATURE
DATE
DRAWN
CHK'D
APPV'D
MFG
Q.A
MATERIAL:
WEIGHT:
TITLE:
Part 6-Outer tube
DWG NO.
A4
SCALE:1:5
SHEET 1 OF 1

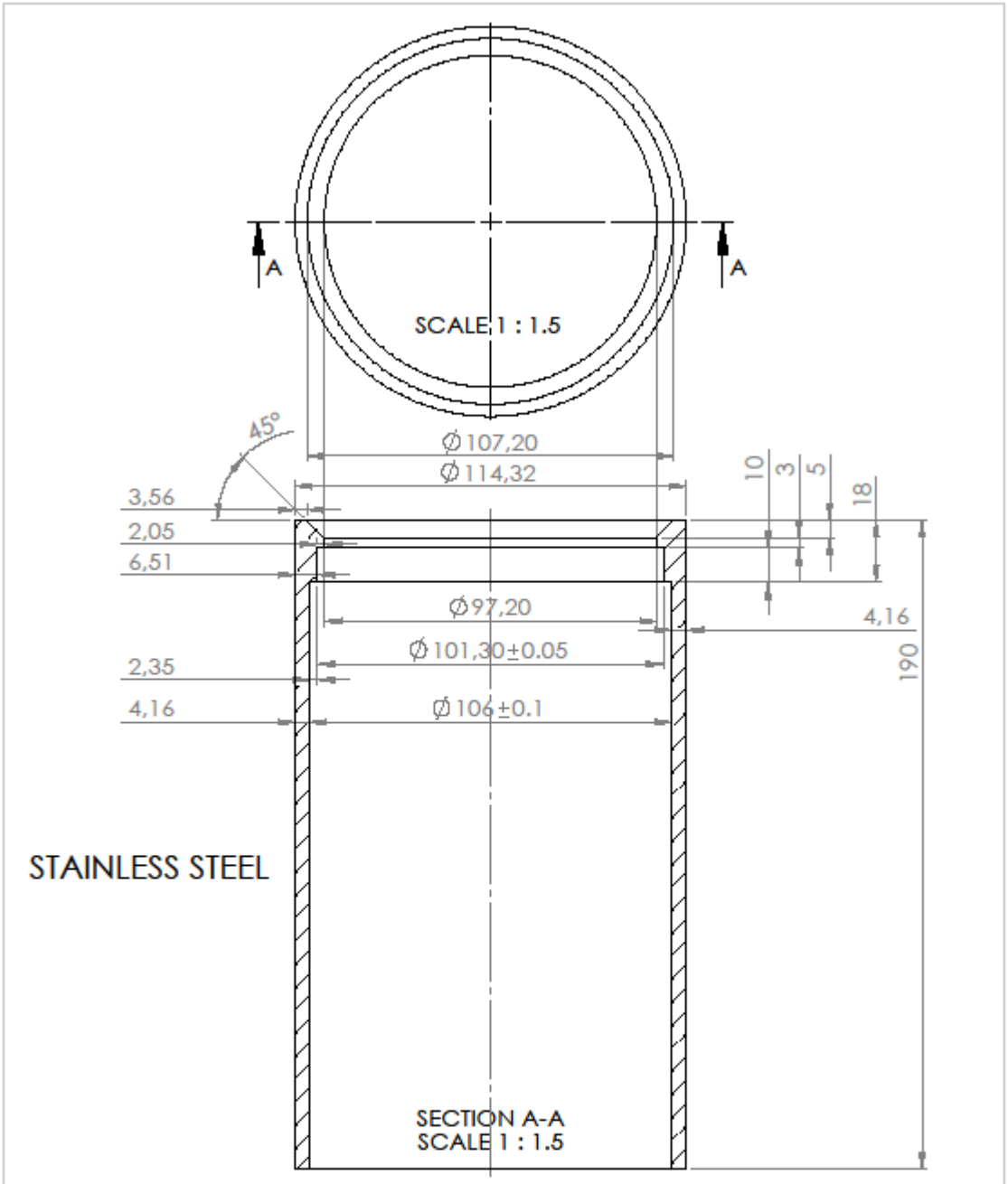

UNLESS OTHERWISE SPECIFIED: DIMENSIONS ARE IN MILLIMETERS SURFACE FINISH: TOLERANCES: LINEAR: ANGULAR:	FINISH:	DEBUR AND BREAK SHARP EDGES	DO NOT SCALE DRAWING	REVISION	
	NAME	SIGNATURE	DATE	TITLE:	
DRAWN				Part 7-Inner tube	
CHK'D					
APPV'D					
MFG					
Q.A			MATERIAL:	DWG NO.	A4
			WEIGHT:	SCALE:1:2	SHEET 1 OF 1

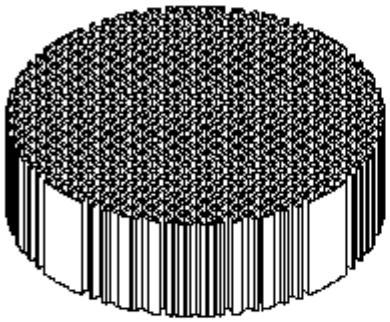

SCALE 1 : 1.5

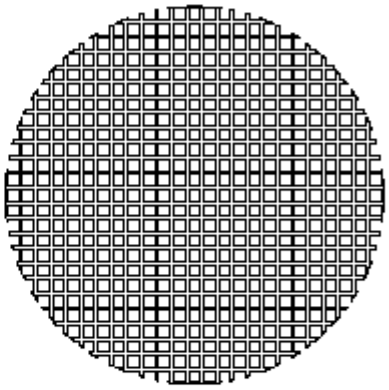

SCALE 1 : 1.5

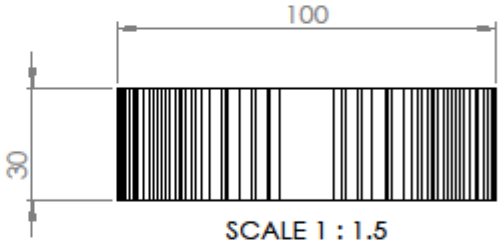

SCALE 1 : 1.5

UNLESS OTHERWISE SPECIFIED: DIMENSIONS ARE IN MILLIMETERS SURFACE FINISH: TOLERANCES: LINEAR: ANGULAR:		FINISH:			DEBUR AND BREAK SHARP EDGES	DO NOT SCALE DRAWING	REVISION
	NAME	SIGNATURE	DATE			TITLE:	
DRAWN						Part 8-Ceramic Absorber	
CHK'D							
APPV'D							
MFG							
Q.A				MATERIAL:		DWG NO.	A4
				WEIGHT:		SCALE:1:2	SHEET 1 OF 1

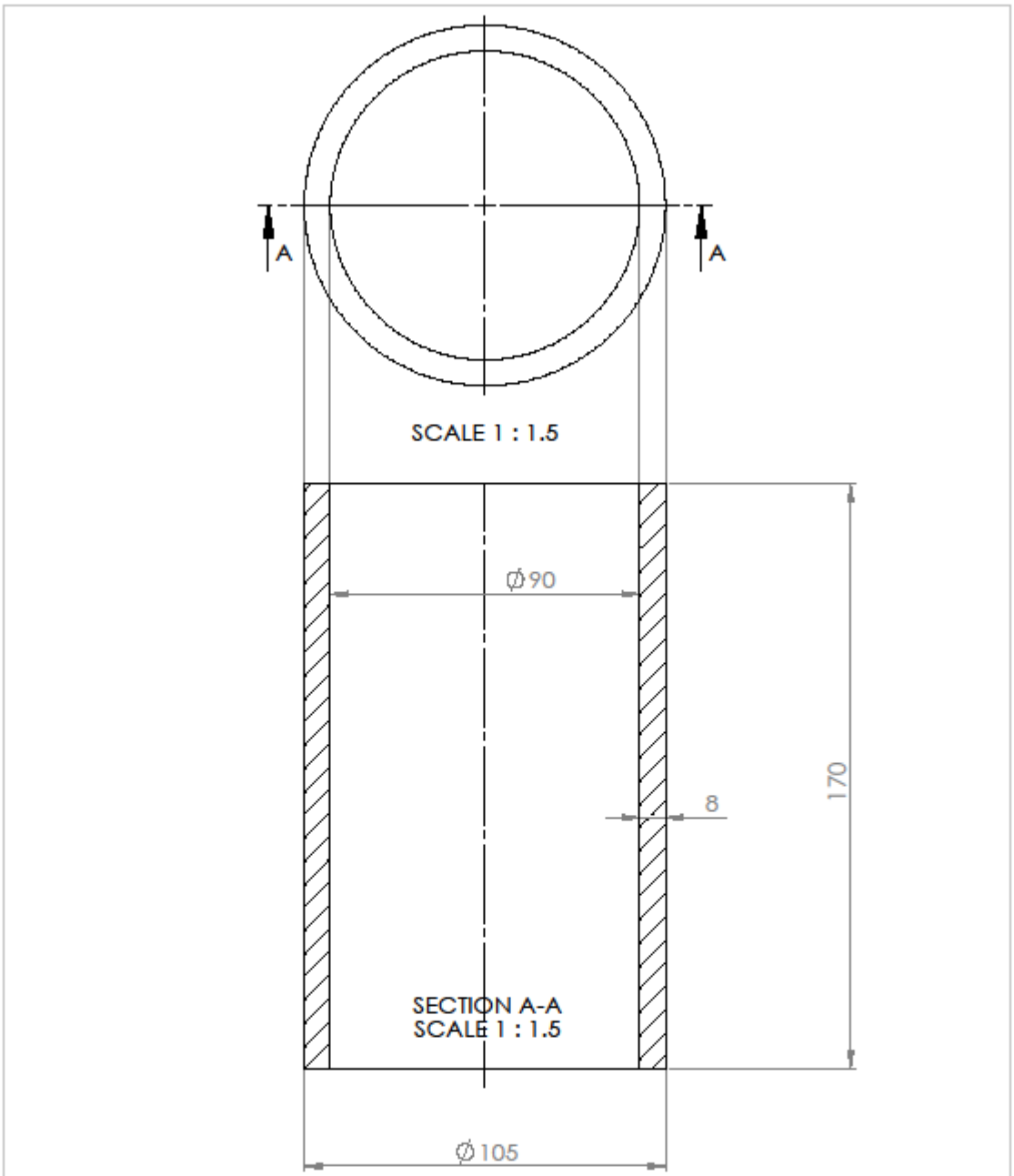

UNLESS OTHERWISE SPECIFIED: DIMENSIONS ARE IN MILLIMETERS SURFACE FINISH: TOLERANCES: LINEAR: ANGULAR:	FINISH:		DEBUR AND BREAK SHARP EDGES	DO NOT SCALE DRAWING	REVISION
	NAME	SIGNATURE	DATE	TITLE:	
DRAWN				Part 9-Ceramic Insulation	
CHK'D					
APPV'D					
MFG					
Q.A			MATERIAL:	DWG NO.	A4
			WEIGHT:	SCALE:1:2	SHEET 1 OF 1

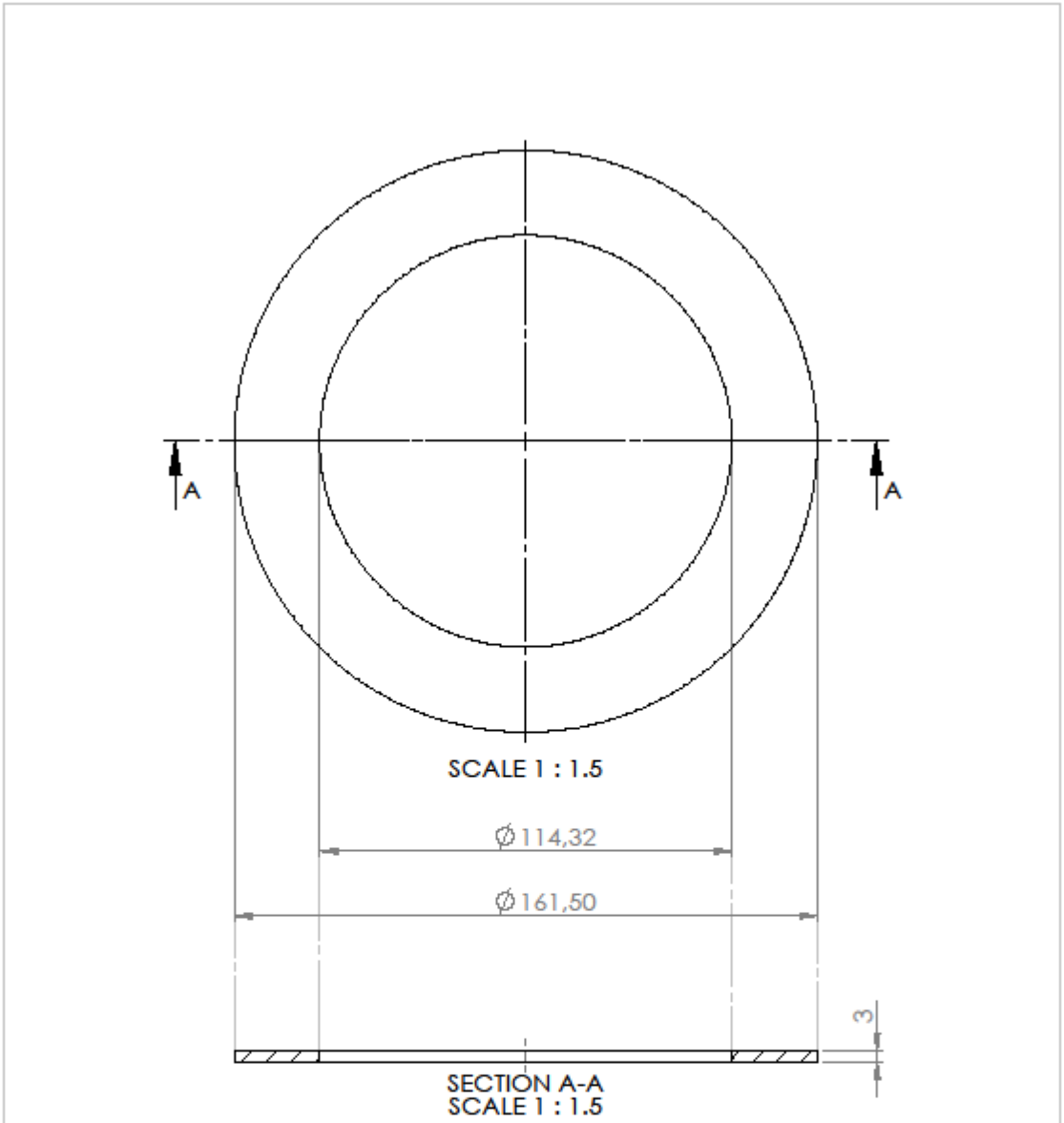

UNLESS OTHERWISE SPECIFIED: DIMENSIONS ARE IN MILLIMETERS SURFACE FINISH: TOLERANCES: LINEAR: ANGULAR:		FINISH:			DEBUR AND BREAK SHARP EDGES	DO NOT SCALE DRAWING	REVISION
	NAME	SIGNATURE	DATE			TITLE:	
DRAWN						Part 10-Bottom cover tube	
CHK'D							
APPV'D							
MFG							
Q.A				MATERIAL:		DWG NO.	A4
				WEIGHT:		SCALE:1:5	SHEET 1 OF 1

SCALE 1 : 1

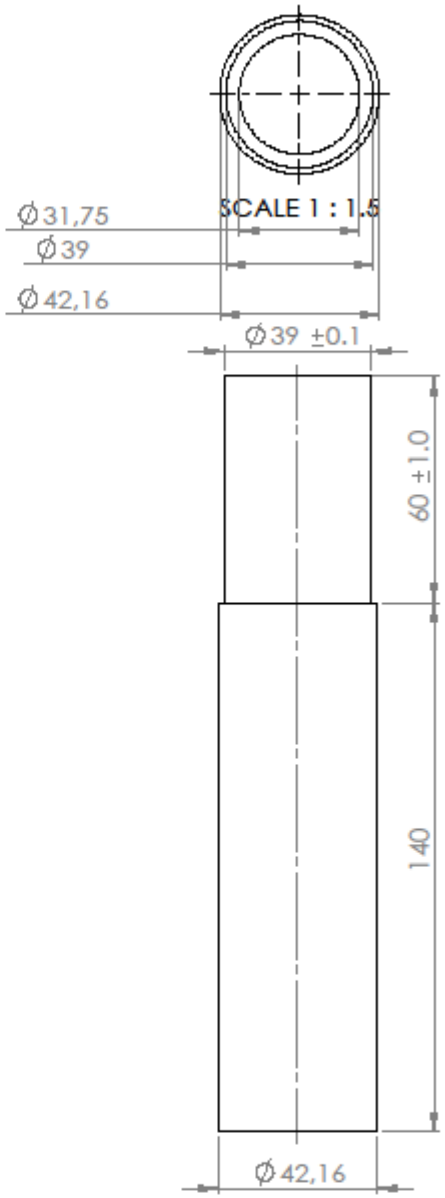

SCALE 1 : 1.5

UNLESS OTHERWISE SPECIFIED: DIMENSIONS ARE IN MILLIMETERS SURFACE FINISH: TOLERANCES: LINEAR: ANGULAR:		FINISH:		DEBUR AND BREAK SHARP EDGES		DO NOT SCALE DRAWING	REVISION
	NAME	SIGNATURE	DATE			TITLE: Part 11-Inlet Pipe	
DRAWN							
CHK'D							
APPV'D							
MFG							
Q.A				MATERIAL:		DWG NO.	A4
				WEIGHT:		SCALE:1:2	SHEET 1 OF 1

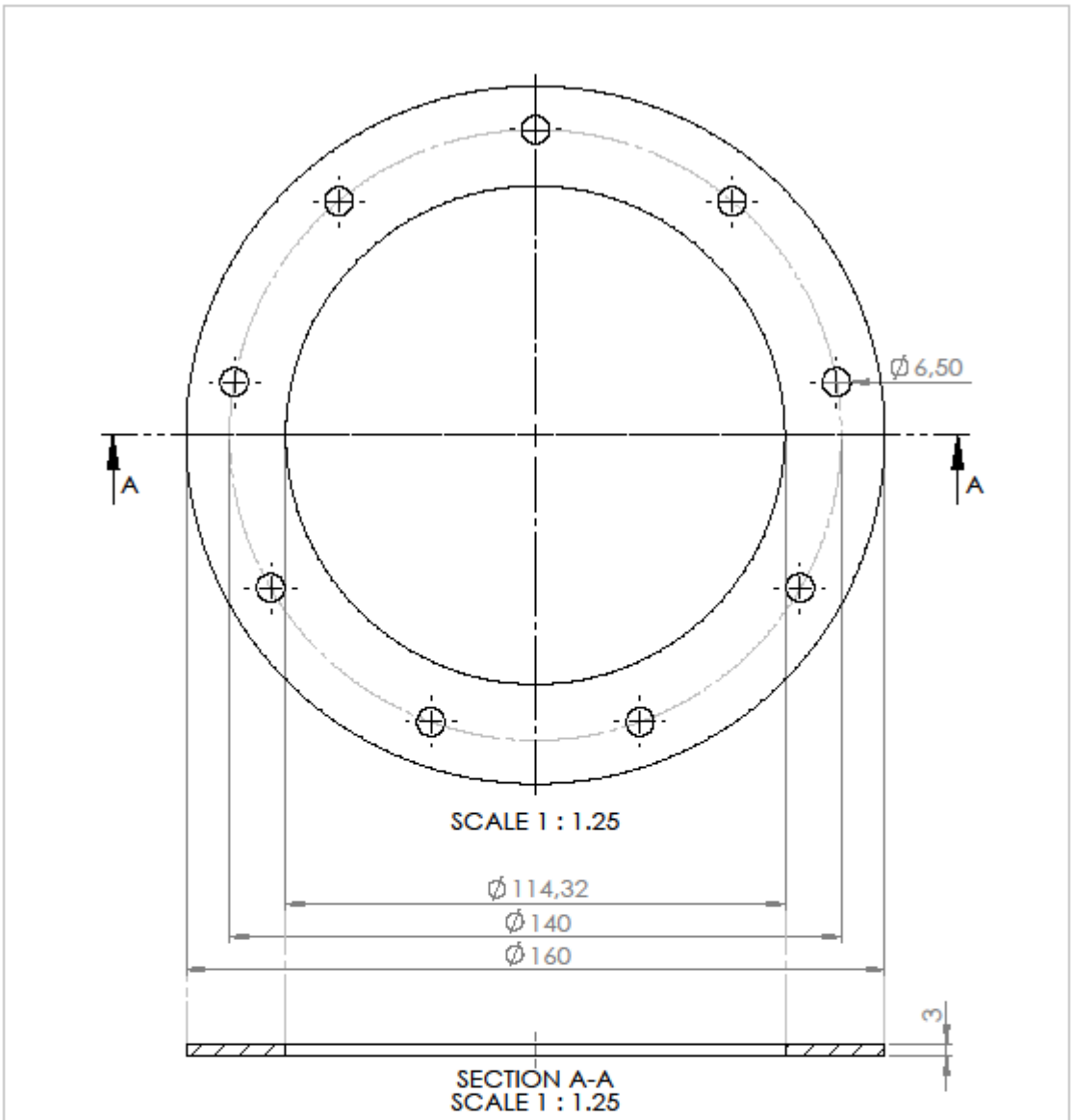

UNLESS OTHERWISE SPECIFIED: DIMENSIONS ARE IN MILLIMETERS SURFACE FINISH: TOLERANCES: LINEAR: ANGULAR:		FINISH:		DEBUR AND BREAK SHARP EDGES		DO NOT SCALE DRAWING	REVISION
	NAME	SIGNATURE	DATE			TITLE:	
DRAWN						Part 12-Ceramic stopper upper part	
CHK'D							
APPV'D							
MFG							
Q.A				MATERIAL:		DWG NO.	A4
				WEIGHT:		SCALE:1:5	SHEET 1 OF 1

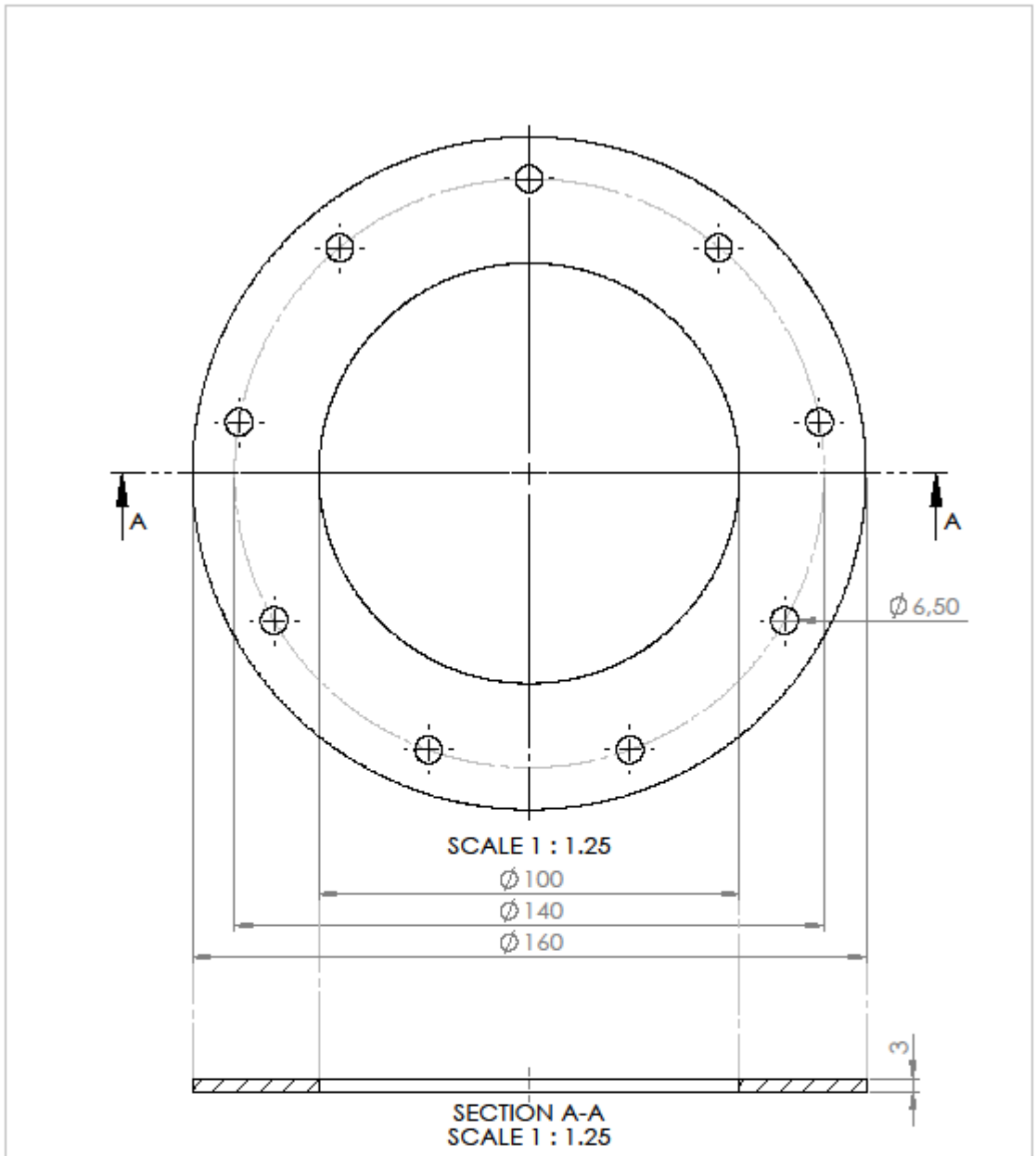

UNLESS OTHERWISE SPECIFIED: DIMENSIONS ARE IN MILLIMETERS SURFACE FINISH: TOLERANCES: LINEAR: ANGULAR:		FINISH:		DEBUR AND BREAK SHARP EDGES		DO NOT SCALE DRAWING	REVISION
	NAME	SIGNATURE	DATE			TITLE: Part 13-Ceramic stopper lower part	
DRAWN							
CHK'D							
APPV'D							
MFG							
Q.A				MATERIAL:		DWG NO.	A4
				WEIGHT:		SCALE:1:5	SHEET 1 OF 1

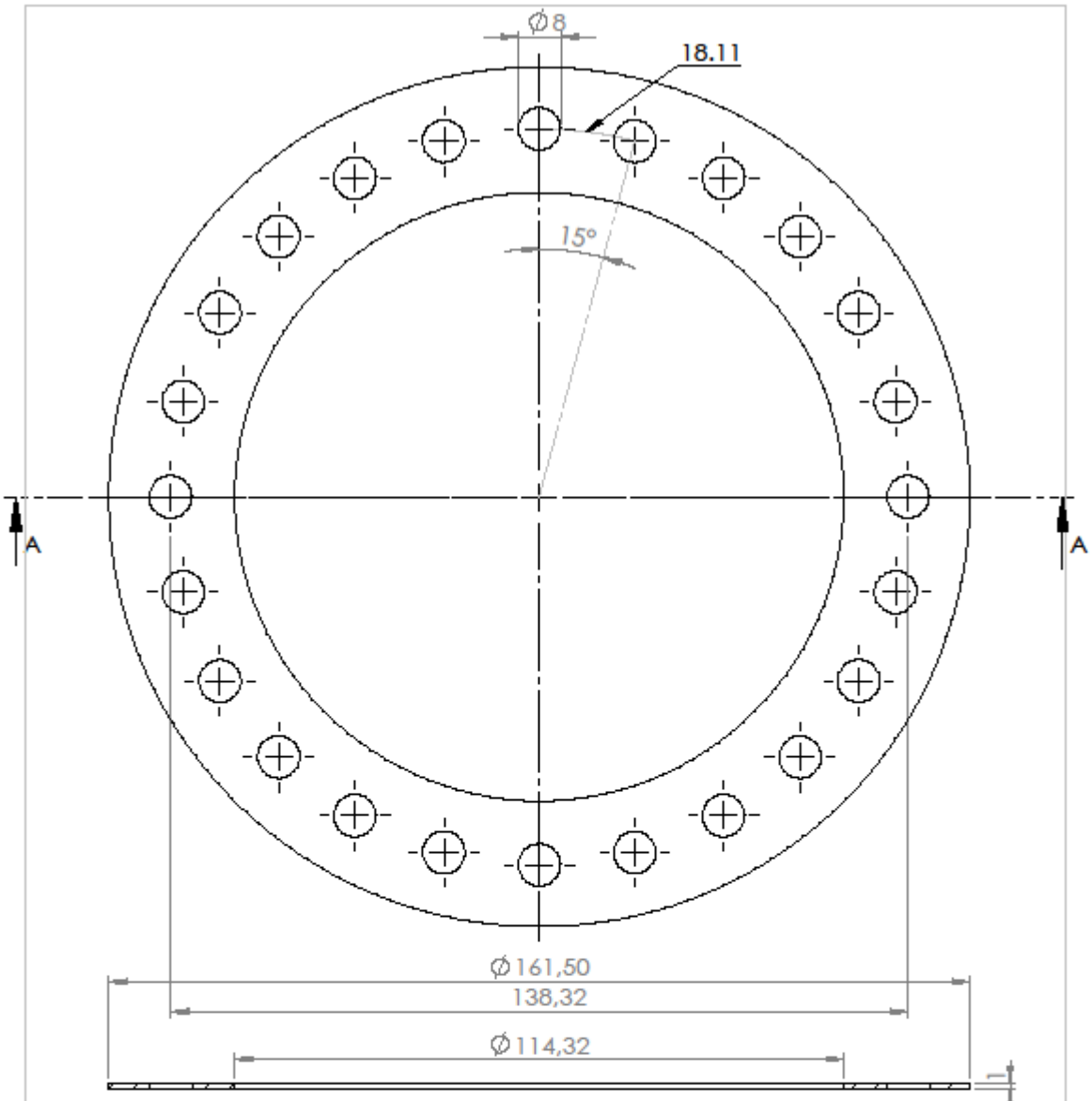

SECTION A-A
SCALE 1 : 1

UNLESS OTHERWISE SPECIFIED: DIMENSIONS ARE IN MILLIMETERS SURFACE FINISH: TOLERANCES: LINEAR: ANGULAR:		FINISH:			DEBUR AND BREAK SHARP EDGES	DO NOT SCALE DRAWING		REVISION
	NAME	SIGNATURE	DATE			TITLE:		
DRAWN						Part 14 - Middle Ring with hole		
CHK'D								
APPV'D								
MFG								
Q.A				MATERIAL:		DWG NO.		A4
				WEIGHT:		SCALE:1:5	SHEET 1 OF 1	

REFERENCES

1. Xu, X., Vignarooban, K., Xu, B., Hsu, K. & Kannan, A. M. Prospects and problems of concentrating solar power technologies for power generation in the desert regions. *Renew. Sustain. Energy Rev.* **53,** 1106–1131 (2016).

2. Buonassisi, T. & Tabet, N. Fundamental of Photovoltaics: The Solar Resource. (2012).

3. Barlev, D., Vidu, R. & Stroeve, P. Innovation in concentrated solar power. *Sol. Energy Mater. Sol. Cells* **95,** 2703–2725 (2011).

4. Barigozzi, G., Bonetti, G., Franchini, G., Perdichizzi, A. & Ravelli, S. Thermal performance prediction of a solar hybrid gas turbine. *Sol. Energy* **86,** 2116–2127 (2012).

5. Sinai, J., Sugarmen, C. & Fisher, U. GT2005-68122 Balance of Plant German Aerospace agency. *Proc. GT2005 ASME Turbo Expo 2005 Power Land, Sea Air June 6-9, 2005, Reno-Tahoe, Nevada, USA* 1–8 (2005).

6. Ávila-Marín, A. L. Volumetric receivers in Solar Thermal Power Plants with Central Receiver System technology: A review. *Sol. Energy* **85,** 891–910 (2011).

7. Smoak, R. H. & Kudirka, A. A. Use of Ceramics in Point-Focus Solar Receivers. in *AIAA 2nd Terrestrial Energy Systems Conference* 1–9 (American Institute of Aeronautics and Astronautics, 1981). doi:10.2514/6.1981-2552

8. Karni, J., Kribus, a., Rubin, R. & Doron, P. The "Porcupine": A Novel High-Flux Absorber for Volumetric Solar Receivers. *J. Sol. Energy Eng.* **120,** 85 (1998).

9. Kribus, A. *et al.* Performance of the Directly-Irradiated Annular Pressurized Receiver (DIAPR) Operating at 20 Bar and 1,200°C. *J. Sol. Energy Eng.* **123,** 10 (2001).

10. Callister, W. D. J. & Rethwisch, D. G. Materials Science and Engineering and Introduction. 46–47 (2010).

11. Fend, T., Pitz-Paal, R., Reutter, O., Bauer, J. örg & Hoffschmidt, B. Two novel high-porosity materials as volumetric receivers for concentrated solar radiation. *Sol. Energy Mater. Sol. Cells* **84,** 291–304 (2004).

12. Kribus, A. *et al.* The promise and challenge of solar volumetric absorbers. *Sol. Energy* **110,** 463–481 (2014).

13. Heller, P. *et al.* Test and evaluation of a solar powered gas turbine system. *Sol. Energy* **80,** 1225–1230 (2006).

14. Sciti, D., Silvestroni, L., Mercatelli, L., Sans, J. L. & Sani, E. Suitability of ultra-refractory diboride ceramics as absorbers for solar energy applications. *Sol. Energy Mater. Sol. Cells* **109,** 8–16 (2013).

15. Sani, E., Mercatelli, L., Francini, F., Sans, J. L. & Sciti, D. Ultra-refractory ceramics for high-temperature solar absorbers. *Scr. Mater.* **65,** 775–778 (2011).

16. Burlafinger, K., Vetter, A. & Brabec, C. J. Maximizing concentrated solar power (CSP) plant overall efficiencies by using spectral selective absorbers at optimal operation temperatures. *Sol. Energy* **120,** 428–438 (2015).

17. GmbH, C. Properties of Ceramic Materials. (2016). Available at: http://www.ceramdis.com/images/content/medien/Properties_ceramic_0316.pdf. (Accessed: 30th April 2018)

18. Rottenbacher, R. & Willmann, G. SiSiC - A Material for High Temperature Ceramic Heat Exchangers. *Ceram. Adv. Energy Technol.* 231–249 (1984).

19. Ceramic, A. I. Data Sheet: Mullite Materials. (2017).

20. Stine, W. B. & Geyer, M. Power From The Sun. (2001). Available at: http://www.powerfromthesun.net/book.html. (Accessed: 11th December 2017)

21. Incropera, F. P., Bergman, T. L., Lavine, A. S. & DeWitt, D. P. *Fundamentals of Heat and Mass Transfer*. *US Patent 5,328,671* (2011). doi:10.1073/pnas.0703993104

22. Dietrich, B. *et al.* Determination of the thermal properties of ceramic sponges. *Int. J. Heat Mass Transf.* **53,** 198–205 (2010).

23. Mendes, M. A. A. *et al.* Measurement and simplified numerical prediction of effective thermal conductivity of open-cell ceramic foams at high temperature. *Int. J. Heat Mass Transf.* **102,** 396–406 (2016).

24. MTPS - C-Therm - Thermal Conductivity Instruments. Available at: http://ctherm.com/products/tci_thermal_conductivity/how_the_tci_works/mtps/. (Accessed: 26th April 2018)

25. Dascomb, J. Low-Cost Concentrating Solar Collector for Steam Generation. *Master Thesis* (Florida State University, 2009).

26. Lovegrove, K. & Stein, W. *Concentrating Solar Power Technology: Principles, developments, and applications*. *Woodhead Publishing Series in Energy: Number 21* (Woodhead Publishing Limited, 2012). doi:10.1533/9780857096173.3.577

27. Lu, T. J. & Fleck, N. A. The thermal shock resistance of solids. *Acta Mater.* **46,** 4755–4768 (1998).

28. Vedula, V. R., Green, D. J. & Hellmann, J. R. Thermal fatigue resistance of open cell ceramic foams. *J. Eur. Ceram. Soc.* **18,** 2073–2080 (1998).

29. Lu, M. C. The Influence of Cyclic Tangential Loading on Indentation Fracture. (University of California, 1984).

30. Adler, J. & Standke, G. SI-SIC LigaFill Foams and Related Net-like Structures - New Lightweight and Low-cost Materials for Spaceborne Applications. 0–6

VITAE

Name	: Ghazi Zulhazmi
Nationality	: Indonesian
Date of Birth	: January 09, 1991
Email	: ghazi.zulhazmi@gmail.com
Address	: Jl. Titiran 2, Blok C-74, Pondok Timur Indah 1, Bekasi, West Java, Indonesia. 17158
Academic Background	: September 2007 – July 2011 B. Eng. in Materials Science and Engineering from Institut Teknologi Bandung, Bandung, Indonesia